PNAS
www.pnas.org

Supplementary Information for

Ostrich eggshell bead strontium isotopes reveal persistent macroscale social networking across late Quaternary southern Africa

Brian A. Stewart*, Yuchao Zhao, Peter J. Mitchell, Genevieve Dewar, James D. Gleason, Joel D. Blum

*Corresponding author: Brian A. Stewart
Email: bastew@umich.edu

This PDF file includes:

Supplementary Text

1. Melikane Rock-Shelter: research history, excavation methods and chronostratigraphy

1.1. Research history

Melikane (1860 m a.s.l.) is a large rockshelter situated along a major tributary of Lesotho's upper Senqu (Orange) River that bears the same name. Formed in Clarens sandstones, the site sits roughly ~70 meters above the Melikane Valley floor. Together with Sehonghong, Melikane is currently the key archaeological sequence in highland Lesotho. Historical sources suggest that both shelters formed important mountain refuges for rapidly disappearing local hunter-gatherer (so-called 'Mountain San') cultures during the nineteenth century[1], and probably also groups of mounted livestock raiders[2] of diverse ethnic composition. Melikane's shelter walls possess particularly important colonial-era paintings that attest to the formation of complex, hybridized new cultural identities during a period of extreme political and socioeconomic upheaval[3]. One of these scenes was recorded 1873 by Joseph Orpen, a member of the punitive Grant expedition[4], who subsequently published them alongside a verbal account of their interpretation by the expedition's Bushman guide, named Qing[5]. These accounts of this scene at Melikane – as well as others at Sehongong and nearby Pitsaneng (where the expedition also camped) – represent some of the only first-hand explanations of the meanings embedded in Bushman rock art.

Melikane was first excavated in 1974 by Pat Carter (University of Cambridge, UK). It was the last of six large shelters (including Sehonghong) that he investigated for a doctoral research project aimed at establishing a basic archaeological sequence for highland Lesotho and the abutting southern uKhahlamba-Drakensberg Escarpment of South Africa[6]. Carter opened an archaeological trench 12 m^2 in area and brought it down to a depth of ~2.6 m below the shelter surface. He recovered an abundance of artifactual material; the levels with Middle Stone Age (MSA)-affiliated cultural materials were particularly prolific. However, samples submitted by Carter for conventional radiocarbon dating from the bottom two-thirds of the sequence returned ages near or beyond the limit of the radiocarbon technique at the time (≥40 ka)[7,] meaning the bulk of Melikane's deposits could not be dated. Moreover, Carter excavated Melikane in artificial 10 cm-thick spits that crosscut the sequence's natural stratigraphy. The resulting lack of chronological and contextual precision made it necessary to return to the site to conduct a more controlled, systematic excavation applying modern stratigraphic and chronometric techniques.

In 2007, a team lead by Zenobia Jacobs (University of Wollongong, Australia) returned to Melikane to re-open Carter's original trench in order to obtain sediment samples for optically stimulated luminescence (OSL) dating. These samples formed part of a broader project to temporally resolve key phases of the southern African MSA[8,9]. The deepest OSL samples at Melikane returned dates of over 80 ka, identifying it as the oldest chronometrically dated deposit in Lesotho. Encouraged by these results, the following year a team led by Brian Stewart (University of Michigan, USA) and Genevieve Dewar (University of Toronto, Canada) returned to Melikane to re-excavate the shelter using modern analytical techniques and a multidisciplinary approach[10]. A new trench 6 m^2 in area was placed a meter east of Carter's original trench, with the long axis oriented parallel to his (Figure S1). The team reached bedrock at a similar depth to Carter at the completion of a second season in 2009. This newer work at Melikane forms part of a larger collaborative project, 'Adaptations to Marginal Environments in the Middle Stone Age' (AMEMSA), co-directed by Stewart and Dewar.

1.2. Excavation methods

Melikane was excavated using a single context recording system with individual stratigraphic units removed according to similarities in color, texture and sedimentary inclusions. For stratigraphic units thicker than 5 cm, excavation proceeded in arbitrary 5 cm-thick spits within the unit. Three cm spits were employed for levels from Layer 18 and below, which are generally thinner (Figure S2). Special finds, faunal remains diagnostic to taxon, and stone tools considered temporally diagnostic were three-dimensionally piece-plotted. Sediments from the upper levels were sieved using 1.5 mm mesh until the high moisture content necessitated a switch to 3 mm mesh. Excavated materials recovered from sieving were preliminarily sorted on-site and packaged for transport to various institutions for specialist analyses. Most, however, are being analyzed at the Museum of Anthropological Archaeology, University of Michigan (where they are also temporarily curated) and the Department of Anthropology, University of Toronto Scarborough. Particularly large and/or well-preserved individual charcoal fragments were collected *in situ* for radiocarbon dating. Bucket flotation was used for sediments from features and other visibly organic-rich deposits in order to obtain larger charcoal and macrobotanical assemblages. The trench was stepped down for safety, with bedrock reached at 2.6 m below the surface in a single square (Square S6). In total, 8.92 m^3 of archaeological deposit was removed over two field seasons.

A total of 12 ostrich eggshell beads were recovered from the Stewart/Dewar excavations at Melikane. All derive from the uppermost Layers 1 and 2, which are radiocarbon dated to the late Holocene (3.3–0.15 ka). The shift to slightly larger (3 mm) mesh size should not have impacted the recovery of ostrich eggshell beads, which across late Pleistocene southern Africa rarely fall below 4 mm in maximum dimension[11]. Rather, the absence of beads in strata deeper than Layer 2 (>24 ka) likely stems from poor organic preservation caused by frequent water ingression. All beads recovered were complete (stage 11 cf. Kandel and Conard[12]). The lack of any other stage of bead manufacture suggests that these beads were not made on site. There are no ostrich eggshell fragments or ostrich bones. Six of the beads have clear wear facets, indicating they were strung and worn for a long period, while a seventh has a heavily worn outer rim. Eleven of Melikane's 12 beads were analyzed in this study (Figure S3).

1.3. Chronostratigraphy

The Melikane sequence excavated in 2008/9 was composed of 45 individual stratigraphic units grouped into 30 layers[10] (Figure S2). The low number of contexts/layers relative to Sehonghong (see SI Appendix, section 2) is a consequence of post-depositional diagenesis of the sediments. There is ample evidence for this at Melikane, particularly in the sequence's upper and central phases (Phases I–IV; Layers 1–16), which include often diffuse interfaces between strata, mottling from *in situ* weathering, high frequencies of rounded to sub-rounded clasts, and diverse microscopic indicators[11,13]. Such chemical transformations are consistent with the presence of two fissures in the rear shelter wall (Figure S1), which link the shelter to an active hydrogeological system. Despite its taphonomic complexities, however, the sequence has produced high-quality evidence for long-term cultural and paleoenvironmental changes across 80 kyr of human history in the highland Maloti-Drakensberg. Particularly encouraging is the generally excellent agreement between the site's cross-correlated AMS radiocarbon and single-grain OSL chronologies[10]. Guided by the resulting geochronology, as well as changes in lithology and lithic technology, six major occupational phases (I-VI) can be distinguished. From top to bottom the phases (and associated layers) recognized in the 2008/9 excavation are:

<u>Phase I</u> (Layers 1–2)
The uppermost levels at Melikane are loose to medium-compacted, dark greyish-brown sandy silts with high ash and charcoal content. Faunal remains here are well-preserved and artifact assemblages diverse. The latter include ostrich eggshell beads, a bone pendant, bone points, freshwater mollusk shells, fire-damaged rock, pottery, ochre fragments, and Later Stone Age (LSA) stone tools of both macro- and microlithic character. Here, as in every phase at Melikane except the earliest (Phase VI), the lithic

assemblage is dominated by high-quality crypto-crystalline silicates (CCS), of which most are amygdaloidal cherts. The northern third of Layer 2 yielded the site's most well-preserved hearth, rock-lined, rich in charcoal and ash, and with much associated bone and seemingly *in situ* lithic knapping scatters. Most radiocarbon dates from Phase I are late Holocene (3.3 ka–0.15 ka) (Table S2) However, an aberrant OSL determination of 8.7 ± 0.7 ka from an equivalent stratum to Layer 2 in Carter's adjacent trench suggests these uppermost sediments have suffered disturbances, likely from bioturbation (Table S2).

Phase II (Layers 3–5)
A series of heavily compacted, yellowish- or goldish-brown silty sands with abundant sub-rounded to rounded sandstone clasts interspersed with much more anthropogenic, very dark brown charcoal-rich sandy silt lenses. The clasts are commonly imbricated in a northerly direction towards the mouth of the shelter, suggesting they represent colluvial influx events whereby exogenous material was introduced into the deposit from rear-wall fissures. Inclusions of sub-rounded burnt bone and charcoal in micromorphological thin-sections, together with the heavily rolled nature of the lithics, suggest these levels represent an intermixing of geogenic and autochthonous anthropogenic sediments as the latter were repeatedly scoured by influxes of the former. Grain size peaks are the highest in the sequence and organic carbon and carbonate contents are consistently low. While efforts to date the uppermost levels (Layers 3–4) have been unsuccessful, an early Last Glacial Maximum age for Layer 5 is indicated by radiocarbon (24.5–23.6 ka) and OSL (27.2 ± 1.8 ka) (Tables S1 and S2). An aberrant radiocarbon date of 3.4–3.2 ka indicates some localized disturbances are present, consistent with several animal burrows visible in section. Lithic assemblages are highly informal early LSA-like in character with frequent *pièces esquillées* and other bipolar products.

Phase IIIa (Layers 6–10)
The strata comprising Phase IIIa are a series of massive sandstone rockfall layers with dark brown sandy silt matrices alternating with coarse colluvial gravels similar to those of Phase II and dark blackish brown, much more anthropogenic levels. Of special note is Layer 8, a blackish brown, extremely charcoal-rich burning stack composed of charred organic material and ash microstrata. Micromorphological analyses of Layer 8 reveal the presence of articulated phytoliths and the preservation of entire plant structures of leaves, stems and charred parenchymous tissue. This burning stack directly overlies the site's largest rockfall horizon (Layer 9) some 10-40 cm in thickness. Stark differences between lithological units in this phase speak to environmental instability, with human occupations interspersed with colluvial ingressions from high-intensity storms and roof-falls from enhanced freeze-thaw action. Radiocarbon samples were subjected to highly rigorous acid-base-wet oxidation stepped-combustion (ABOx-SC) pretreatment to eliminate contamination. Both those and OSL samples taken from Phase IIIa returned ages of mid-Marine Isotope Stage (MIS) 3 (42.6–36.3 ka and 41.3 ± 3 ka, respectively) (Tables S1 and S2). A final aberrant date of 0.45–0.3 ka for Layer 6 suggests bioturbation reached into this uppermost level of Phase III, but not deeper. Lithic assemblages here are a mix of informal flake and core technologies together with rarer diagnostic MSA elements, blades and bladelets.

Phase IIIb (Layers 11–16)
This sub-phase shares similarities in both age and sedimentological character to overlying IIIa, though some important differences merit its partition. While rockfall is present (and sometimes substantial), deposition of colluvial gravel layers that become so conspicuous in Phases IIIa and II had not yet begun. Instead, Phase IIIb is dominated by mottled, yellowish brown/black sandy silt layers (Layers 12 and 14) with sporadic large-medium roof-fall slabs and occasional scree. Interspersed between these mottled levels are a series of thinner (≤4 cm), more charcoal-rich anthropogenic horizons (Layers 11, 13 and 15). Moreover, the Phase IIIb lithic assemblages contain a higher proportion of both blades and typical MSA forms than those of overlying IIIa. Radiocarbon dates suggest IIIb occurred immediately before IIIa; traditional acid-base-acid (ABA)-pretreated ages (Layers 10 and 12) are statistically indistinguishable from those from IIIa, but the sole sample to survive ABOx-SC (from Layer 14) returned an age of 43.0–40.7 ka (Table S1). This agrees

statistically with an OSL age from an equivalent stratum in Carter's adjacent trench (45.9 ± 3.8 ka) (Table S2). Another OSL sample for Phase IIIb's deepest unit, Layer 16, produced a stratigraphically inverted age of 53.8 ± 3.2 ka that seems erroneously old. Together, Phases IIIa and b add up to over one meter of stratigraphy, which means that over one-third of the 2.6 m Melikane sequence was deposited in less than ~10 kyr (~46-37 ka) (Figure S2).

Phase IV (Layers 17–21)
The sediments comprising this phase and those below it (V and VI) were deposited under less volatile conditions, when Melikane was a younger, less energetic rock shelter. Alternating layers of dark yellowish brown, dark blackish brown and yellow/black mottled sandy silts characterize these strata, with variably high content of small, rounded clasts ('pea gravel') and infrequent small sandstone slabs. Contacts between stratigraphic units are sharper than above, though micromorphological observations suggest that water throughput dissipated internal microstratigraphy. Amorphous iron staining of lithics also indicates the strong influence of water, and sparitic calcitic coatings may reflect the dissolution and re-precipitation of calcium carbonate from ash. Lithic technologies of Phase IV are distinctly more MSA in character, with convergent flakes struck from small Levallois cores a conspicuous component. Attempts to pretreat radiocarbon samples with ABOx-SC failed at this depth. Two samples with standard ABA pretreatment produced ages of 49.6–43.7 ka (Layer 20) and 43.3–41 ka (Layer 19). These are almost certainly too young for this phase, though the former approaches its probable age as suggested by a single OSL age of 50 ± 1.9 ka for a Carter level equivalent to Layer 20.

Phase V (Layers 22–25)
A series of very dark to blackish brown sandy silt levels that are charcoal-rich for this depth and heavily anthropogenic. The sediments possess a slightly higher pea gravel content and more frequent, sub-angular small sandstone slabs and spalls than Phase IV. Here we are beyond the 'radiocarbon ceiling'. Instead, these levels are dated by a single OSL determination of 61 ± 2.5 ka from a Carter level equivalent to Layer 23 (Table S2). While it is possible that this date does not capture the full span of Phase V, a late MIS 4 age it is consistent with its lithic assemblages. These include elements typical of the Howiesons Poort technocomplex, including numbers of backed artifacts and high frequencies of sinuous blades struck from single platform cores. Phase V and underlying Phase VI were only reached in Square S6.

Phase VI (Layers 26–30)
The basal levels at Melikane consist of very dark to blackish brown clayey silts with small, sub-angular gritty clasts. Yellow mottling and associated degraded sandstone spalls increase down-sequence, culminating in the deepest unit, Layer 30, which is composed largely of decomposed bedrock and is culturally nearly sterile. Two statistically overlapping OSL determinations of 79.5 ± 3.1 ka and 83.2 ± 6.2 ka were obtained for Carter equivalents of Layers 28 and 30, respectively (Table S2). These ages are the earliest chronometric dates thus far obtained for Lesotho and suggest that the earliest human occupations at Melikane occurred during the closing millennia of MIS 5, during sub-stage 5a. The Phase VI lithic assemblages differ from all deposited afterwards in being dominated by relatively coarse-grained silicified sandstones rather than CCS. Opposed platform blade cores and informal multidirectional cores are typical, with long blades very common and tool forms dominated by borer/perforators and diverse scrapers. There is extensive evidence of soft-hammer percussion.

Figure S1. Site photographs of Stewart/Dewar 2008/9 (AMEMSA) excavations at Melikane. **a)** Excavation in process of Layer 2 (late Holocene) with large rock-lined hearth emerging in foreground. **b)** Excavation in process of mottled, sandstone-rich Layer 16 (mid-MIS 3). **c)** Position of project AMEMSA's 2008/9 trench in relation to Carter's original 1974 trench (backfill of latter partially removed). Note fissures in shelter rear wall.

Table S1. Radiocarbon dates obtained from Stewart/Dewar excavations at Melikane Rock-Shelter.

Layer	Context/spit	Laboratory number	14C BP (ABA)	Cal BP* (95.4%) (ABA)	Laboratory number (ABOx-SC)	14C BP (ABOx-SC)	Cal BP* (95.4%) (ABOx-SC)	Material	Reference
1	2/1	OxA-22965	254 ± 22	307–151	-	-	-	Charcoal	Stewart et al.[10]
2	2/2	OxA-22968	270 ± 22	319–152	-	-	-	Charcoal	Stewart et al.[10]
2	2/3	OxA-22966	3047 ± 27	3336–3071	-	-	-	Charcoal	Stewart et al.[10]
3	4/1	OxA-22967	207 ± 22	295–11	-	-	-	Charcoal	Stewart et al.[10]
3	4/2	OxA-22837	445 ± 22	507–338	-	-	-	Charcoal	Stewart et al.[10]
5	7(6-8)/1	OxA-23028	20000 ± 190	24469–23546	-	-	-	Charcoal	Stewart et al.[10]
5	6-8/2	OxA-22838	3112 ± 25	3366–3181	-	-	-	Charcoal	Stewart et al.[10]
6	9/75-80	OxA-22963	333 ± 23	448–301	-	-	-	Charcoal	Stewart et al.[10]
6	9/80-85	OxA-23040	32040 ± 370	36736–35042	OxA-23039	33070 ± 380	38331–36272	Charcoal	Stewart et al.[10]
7	10/90-95	OxA-23032	35400 ± 900	41871–38323	OxA-23041	37200 ± 1600	45032–38740	Charcoal	Stewart et al.[10]
8	11/85-90	OxA-22964	35600 ± 450	41218–39160	OxA-23035	36250 ± 700	42076–39457	Charcoal	Stewart et al.[10]
8	11/90-95	OxA-22839	34190 ± 390	39689–37613	OxA-23033	36700 ± 800	42525–39745	Charcoal	Stewart et al.[10]
8	11/95-100	OxA-23029	34200 ± 750	40422–36629	-	-	-	Charcoal	Stewart et al.[10]
9	12/100-105	OxA-22791	33950 ± 700	39990–36475	OxA-23034	37300 ± 550	42568–40812	Charcoal	Stewart et al.[10]
10	18/110-115	OxA-22792	34000 ± 700	40052–36521	-	-	-	Charcoal	Stewart et al.[10]
12	15A	OxA-23030	33200 ± 1200	40496–34963	-	-	-	Charcoal	Stewart et al.[10]
14	17/160-165	OxA-23031	34150 ± 650	40141–36770	OxA-23036	37550 ± 700	42964–40771	Charcoal	Stewart et al.[10]
19	20/180-185	OxA-22794	37900 ± 750	43332–41022	-	-	-	Charcoal	Stewart et al.[10]
20	21	OxA-22793	42600 ± 1600	49587–43701	-	-	-	Charcoal	Stewart et al.[10]

***** Calibrated with OxCal v. 4.2[14] using the latest SHCal13 calibration curve for the Southern Hemisphere[15]

Table S2. Optically stimulated luminescence (OSL) dates obtained from Carter tranch at Melikane Rock-Shelter and relationship to adjacent Stewart/Dewar layers (after Stewart et al.[10], Table 3).

Carter Layer	Stewart/ Dewar Layer equiv.	Sample code	Moisture content (%)	Dose rates (Gy/ka)			Total dose rate [d,e]	D_e (Gy)[f]	Age model	Proportion (%)	Number of grains [g]	Overdisp. (%)[h]	OSL age (ka)[i]
				Beta[a]	Gamma[b]	Cosmic [c]							
1	2	MLK10	12 ± 2	1.20 ± 0.08	0.78 ± 0.02	0.09	2.11 ± 0.11	6.7 ± 0.4 **18.3 ± 1.0** 47.9 ± 5.4	FMM1 **FMM2** FMM3	29.3 **55.6** 15.1	112 / 1900	70 ± 5	3.2 ± 0.3 **8.7 ± 0.7** 22.7 ± 2.9
3	5	MLK9	13 ± 2	1.31 ± 0.08	0.93 ± 0.02	0.09	2.36 ± 0.13	37.2 ± 1.4 **64.0 ± 1.7** 108.4 ± 5.5	FMM1 **FMM2** FMM3	19.6 **61.8** 18.6	189 / 1000	41 ± 3	15.7 ± 1.1 **27.1 ± 1.8** 45.9 ± 3.6
4a	8	MLK8	19 ± 5	1.05 ± 0.09	1.07 ± 0.02	0.09	2.24 ± 0.14	51.0 ± 4.5 **92.2 ± 2.8** 135.4 ± 6.5	FMM1 **FMM2** FMM3	5.4 **66.0** 28.6	215 / 900	26 ± 2	22.8 ± 2.5 **41.3 ± 3.0** 60.6 ± 4.9
5 (upper)	14	MLK6	19 ± 5	1.41 ± 0.10	0.91 ± 0.02	0.09	2.45 ± 0.16	61.8 ± 4.8 **112.7 ± 5.1** 163.0 ± 10.1	FMM1 **FMM2** FMM3	8.0 **61.4** 30.6	157 / 1000	29 ± 2	25.2 ± 2.6 **45.9 ± 3.8** 66.5 ± 6.2
5 (lower)	16	MLK5	19 ± 5	1.37 ± 0.09	0.81 ± 0.02	0.09	2.30 ± 0.15	**123.6 ± 8.1** 186.9 ± 24.9	**FMM1** FMM2	**66.4** 33.6	225 / 900	28 ± 2	**53.8 ± 3.2** 81.4 ± 12.2
6 (upper	20	MLK4	19 ± 2	1.15 ± 0.03	0.69 ± 0.04	0.08	1.95 ± 0.05	**97.4 ± 1.8**	**CAM**	100	103 / 800	14 ± 2	**50.0 ± 1.9**
6 (central)	23	MLK3	19 ± 2	1.21 ± 0.03	0.78 ± 0.04	0.08	2.10 ± 0.05	**128.1 ± 3.0**	**CAM**	100	64 / 1000	9 ± 3	**61.0 ± 2.5**
6 (lower)	28	MLK2	19 ± 2	1.33 ± 0.04	0.87 ± 0.05	0.08	2.31 ± 0.06	**183.7 ± 3.8** 70.0 ± 13.5	**FMM1** FMM2	97 3	251 / 1000	25 ± 2	**79.5 ± 3.1** 30.3 ± 5.9
7	30	MLK1	19 ± 5	1.60 ± 0.12	0.92 ± 0.03	0.08	2.63 ± 0.17	**218.8 ± 7.3**	**CAM**	**100**	40 / 1000	21 ± 5	**83.2 ± 6.2**

[a] Measurements made on sub-samples of dried, homogenised and powdered samples by GM-25-5 beta counting. Dry dose rates calculated from these activities were adjusted for the estimated long-term water content water content and for the effects of grain size and hydrofluoric acid etching on beta dose attenuation[16,17].

[b] Measurements made using *in situ* gamma spectrometry. The measured (field) dose rates were adjusted for the water content. The field moisture contents ranged between 12 and 25%. Ages increase by ~1% for each 1% increase in water content.

[c] Cosmic-ray dose rates have been calculated using the equations provided by Prescott and Hutton[18], taking into account site latitude (-29.6 °S), longitude (28.8 °E) and altitude (1850 m). We have also accounted for the density and thickness of overlying sandstone roof and sediment overburden, and for the $\cos^2$-Φ zenith angle dependence of cosmic rays[19]. Dry dose rates were also adjusted for water content[20].

[d] Mean ± total uncertainty (68% confidence interval), calculated as the quadratic sum of the random and systematic uncertainties.

[e] Includes an assumed internal alpha dose rate of 0.03 ± 0.01 Gy/ka.

[f] Estimated from single grains of quartz using the Finite Mixture Model (FMM) or Central Age Model (CAM).

[g] Number of individual grains used for D_e determination / total number of grains analysed.

[h] Overdispersion, the relative standard deviation of the D_e distribution after allowing for measurement uncertainties[21].

[I] Total uncertainty includes a systematic component of ± 2% for possible bias associated with laboratory beta-source calibration.

Figure S2. Section drawing of Melikane stratigraphic sequence – west wall of the AMEMSA trench.

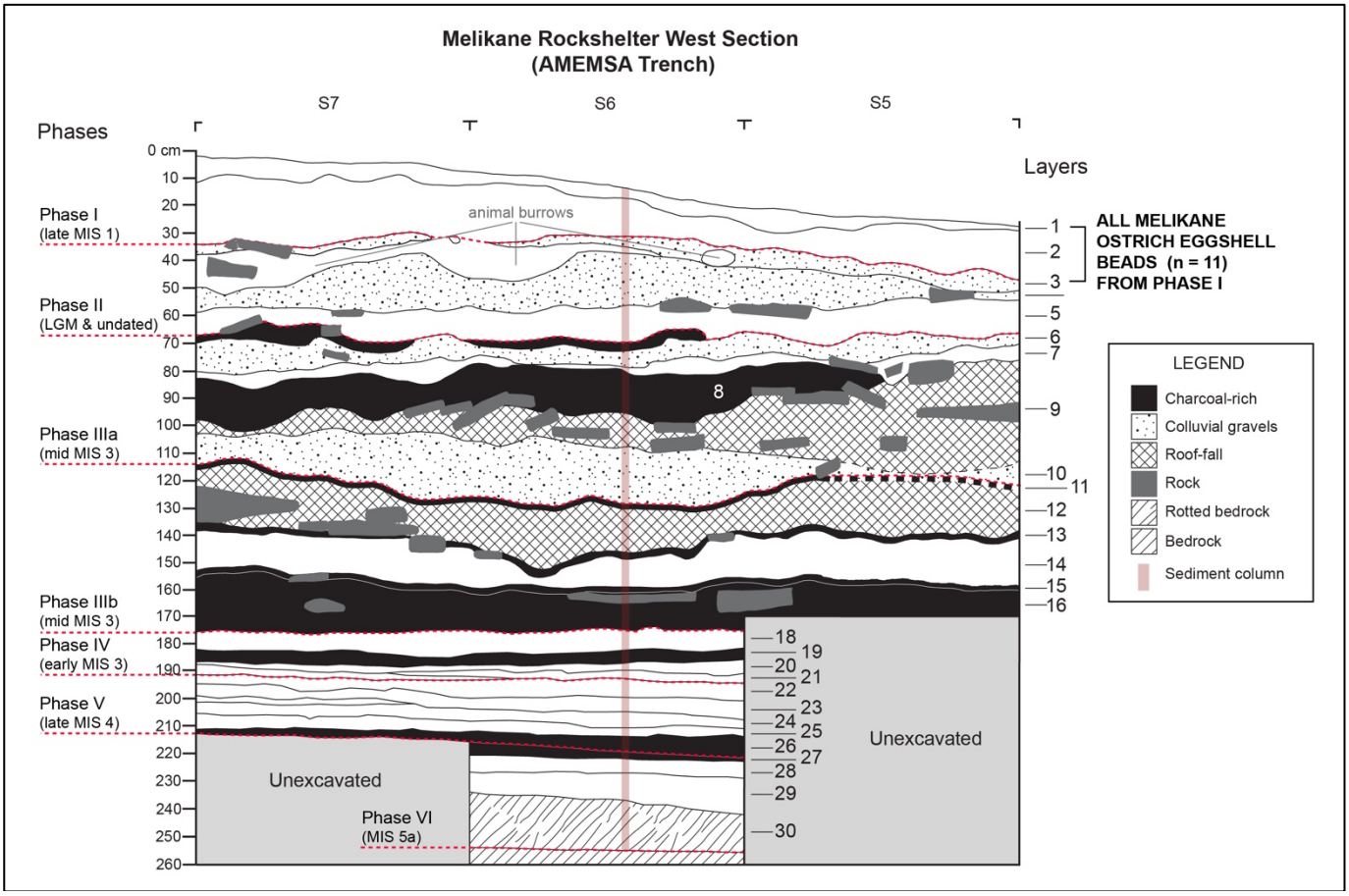

Figure S3. Photographs of ostrich eggshell beads sampled from Melikane.

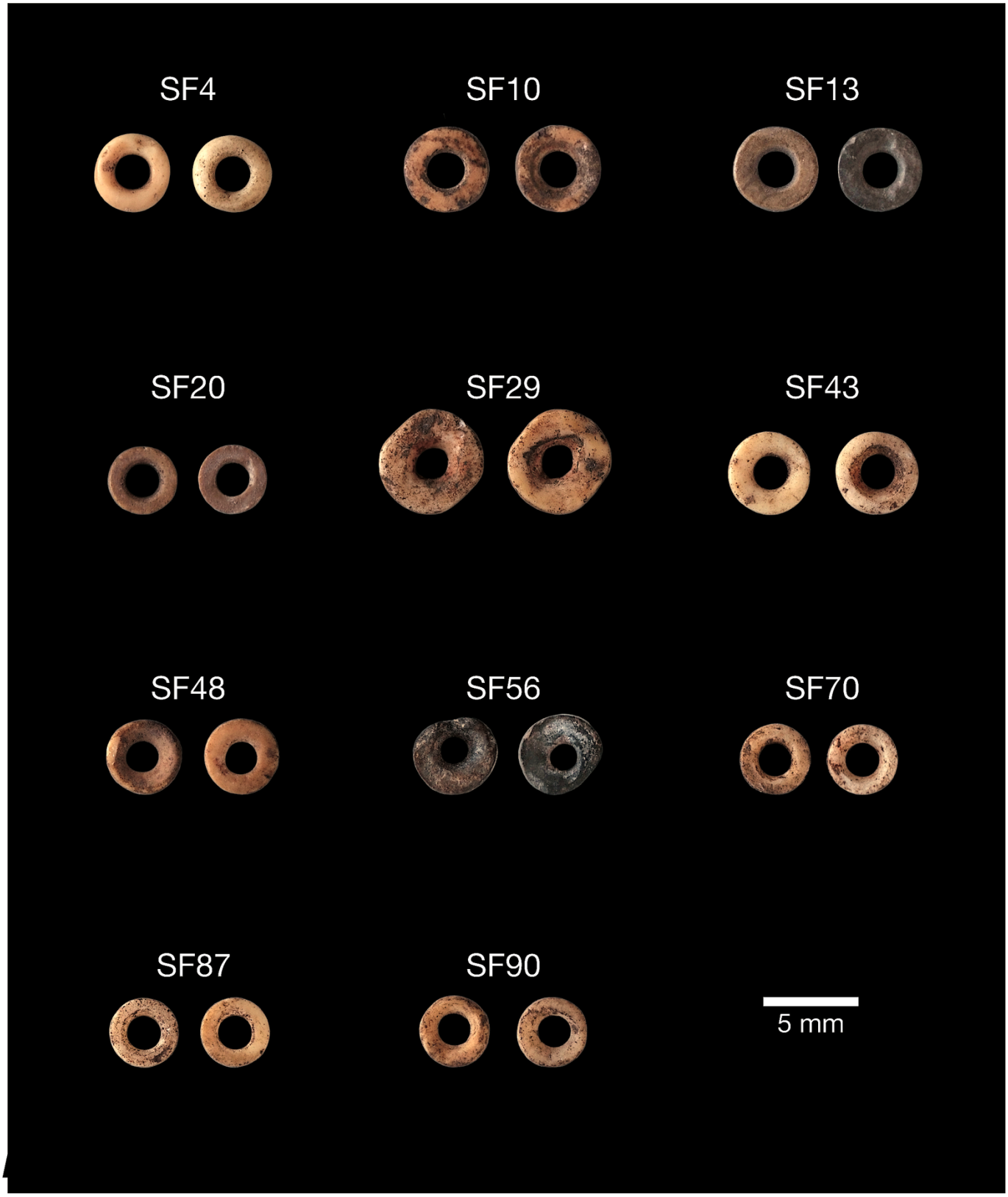

2. Research history, excavation methods, and chronostratigraphic details for Sehonghong Rock-Shelter

2.1. Research history

Sehonghong (1800 m a.s.l.) is the largest rockshelter along the upper reaches of Lesotho's Senqu (Orange) River. Similar to Melikane, the site is formed in Clarens sandstones and located along another major eastern tributary of the Senqu (the Sehonghong River). The shelter's position within the valley differs from Melikane, however, since it is situated only roughly five meters above the valley floor. Its rich, though now poorly conserved, series of rock paintings includes a well-known scene showing the capture of two 'rain-animals' first recorded by Joseph Orpen[5]. One of only three scenes interpreted by a Bushman informant from a population still engaged in producing paintings, these images, like those at Melikane, played a critical part in developing current understandings of southern African hunter-gatherer rock art[22]. The site was inhabited by Bushmen until shortly before Orpen's 1873 visit and then again by a few Bushman individuals until the dawn of the twentieth century[23,24].

Sehonghong was first excavated in 1971 by Patrick Carter, who removed the deposit to bedrock in its most sheltered, northeastern corner, uncovering a sequence of Middle Stone Age (MSA) and Later Stone Age (LSA) occupations extending from about 59 kya[9] into the second millennium AD[6,25,26]. However, because his excavations employed 10 cm-thick horizontal spits that cut across the site's natural stratigraphy, the site's LSA sequence (spanning Marine Isotope Stage (MIS) 2 and the Holocene) was subsequently re-investigated in 1992 by Peter Mitchell (University of Oxford, UK) (Figure S4)[27]. Current excavations by Brian Stewart (University of Michigan, USA) and Genevieve Dewar (University of Toronto, Canada) are extending this excavation down into underlying MSA layers (Figure S4)[28]. All beads analyzed in this study come from the Mitchell and Stewart/Dewar excavations.

2.2. Excavation methods

Mitchell's 1992 excavations employed observable distinctions in their color, texture and inclusions to remove individual sedimentary contexts following the site's natural stratigraphy. Excavation ceased on reaching a rockfall event known from Carter's[6] earlier work to date to close to the boundary between MIS 2 and 3. All excavated deposit was sieved through a 1.5 mm mesh on-site, except for that from the uppermost horizons, DC and SS (Table S3, Figure S5), for which a 3 mm mesh was employed. Finds were sorted on-site and artifacts subsequently analyzed at the Department of Archaeology, University of Cape Town, South Africa. A total of 523 ostrich eggshell beads was retrieved, along with 23 fragments (5.2 g) of unworked ostrich eggshell. Fifteen of these beads were analyzed in this study. Bones attributable to ostrich were restricted to the mid-Holocene layers ALP and GWA (a long bone shaft and a femur head respectively) and the immediately pre-Last Glacial Maximum layer BAS (a wing bone)[29].

Stewart and Dewar's excavations have continued downward within the same trench as that excavated by Mitchell, investigating the MSA levels that form the bottom three-fifths of Sehonghong's deposits. Sedimentary contexts were again removed following observable differences in soil color, texture and inclusions. All artifacts ≥2.5 cm in maximum dimension were individually piece-plotted and all sediments sieved through a 1.5 mm mesh. Bucket flotation was used for sediments from features and other visibly organic-rich deposits in order to obtain larger charcoal and macrobotanical assemblages. Though specialists from a range of institutions are working on various assemblages, most artifacts are being analyzed at either the Museum of Anthropological Archaeology, University of Michigan (where they are also temporarily curated) or the Department of Anthropology, University of Toronto Scarborough. A small number of ostrich eggshell beads have been retrieved from the MSA levels excavated to date. One, recovered *in situ* as a

plotted artifact in Context 170 (bracketed 33.7–31.9 ka), was included in this study, bringing the total number of ostrich eggshell beads analyzed from Sehonghong to 16 (Figure S6).

2.3. Chronostratigraphy

The deposit excavated at Sehonghong in 1992 comprised a total of 174 separate stratigraphic contexts that were subsequently grouped together into 13 layers for the purposes of analysis (Table S3, Figure S5)[30–33]. Where recent application of AMS ^{14}C dating to some of these contexts suggests that they should be reassigned to a different layer this is noted below. Table S3 lists all available radiocarbon dates available for the Mitchell/Stewart/Dewar trench. From top to bottom the layers recognized in the 1992 excavation are:

SS (Surface Scrapings)
Loose grey-brown dust lying on the site's surface with a high modern dung content, plus occasional maize cobs, peach stones, and pieces of paper. LSA artefacts are few and clearly derive from immediately underlying layers.

DC (Dung Crust)
A hard, friable, grey layer mostly consisting of cattle (and some horse) dung, coming away in large lumps, but much finer and ashier with markedly less dung toward the base. Four radiocarbon dates suggest that much of the material present may derive from a time-limited horizon c. 1.25-1.13 kya[32,34], although the layer clearly continued to accumulate into the nineteenth, and likely twentieth, centuries.

GAP (Grey Ash with Pottery)
A soft, loose, light grey, charcoal-rich ashy layer found only in the western half of the 1992 trench. A pit formerly assigned to this layer and associated with charcoal yielding a date of 1240 ± 50 BP (Pta-6084) is now considered to be part of DC. Two further radiocarbon dates place GAP in the early/mid-portion of the first millennium cal. AD.

GWA (Grey White Ash)
A series of quite firm white to pinkish-white ashy bodies with high charcoal content that are probably the remains of interlensing hearths. Present only in the eastern half of the 1992 excavation, GWA is dated on charcoal to 6.9-6.6 kya[33], but a bone date from Layer DC of 6.7-6.5 kya must also derive from GWA, with the sample in question having been displaced upward[34].

ALP (Ashy Loams with Plants)
A series of predominantly reddish-brown or black ashy contexts, many containing partly humified plant remains, some with a distinctly more ash-rich content, especially toward the layer's base and the rockshelter's rear wall. Four conventional radiocarbon dates date ALP to 8.3-7.7 kya,

SA (Sandy Ash)
Mottled orange-brown sandy contexts, most strongly developed toward the western, front end of the excavation, whereas firmer, white ashy contexts occur toward the rear. The topmost contexts of this layer were partially calcreted and constitute a clear break with the base of Layer ALP. The layer is dated to 11.6-10.3 kya.

BARF (Beige Ash above Rock Fall)
A thin, beige-coloured ash containing partly decayed fine grass material interpreted as bedding and found only in the western end of the excavation trench. BARF's single radiocarbon date has an unhelpfully wide standard error, indicating that its age is most likely 13.4-12.6 kya.

RF (Rock Fall)

This layer contains a high number of sandstone fragments derived from at least three rockfall events that probably took place in close succession and are interstratified with a black, organic-rich soil with excellent macroplant preservation. AMS dates place Layer RF at 14.9-13.8 kya, consistent with a conventional date from the 1992 excavation and two dates on bone from Carter's 1971 excavation. Two conventional dates previously attributed to the underlying layer RBL/CLBRF from the 1992 excavation (Pta-6058, Pta-6062) are now reassigned to RF.

RBL/CLBRF (Red Brown Loam/Carbonaceous Loams Below Rock Fall)
This layer comprises a brown, compost-like light loamy soil with a high macroplant content but few sandstone inclusions and a series of ashy, sometimes very charcoal-rich contexts present only at the eastern (rear) end of the excavation. Two AMS dates bracket this layer at 15.7-15.2 kya, with older charcoal and bone determinations from Carter's excavation having much larger standard errors.

BAS (Brown Ashy Sand)
A fine, loose, grey/brown, ashy sand, the bulk of which likely dates to 24.7-22.8 kya, but with evidence of at least two minor subsequent occupation events after the Last Glacial Maximum around 22.3-20.8 kya and 19.3-18.6 kya.

OS (Orange Sand)
A thin, almost culturally sterile orange sand with a high number of small sandstone roof spalls that is the direct equivalent to Layer VIII of Carter's excavation. A radiocarbon date of 20,100 ± 90 BP (OxA-32917) brackets OS at 24.4-23.9 kya, although a second AMS date (OxA-32916) is clearly and inexplicably out of sequence.

MOS (Mottled Orange Sand)
A series of brown to orange sandy contexts, some with small sandstone spall inclusions, that have extensive darker brown or black mottling derived from the presence of charcoal or decayed macroplant remains. This layer corresponds directly to Layer VII of Carter's excavation. MOS is dated to 25.3-23.8 kya, but recently obtained AMS dates suggest that this bracket may be rather tighter at 25.0-24.1 kya.

RFS (Rock Fall with Sand)
A major episode of roof collapse associated with numerous, thin sandstone spalls and angular rocks, mostly <40 cm in maximum size, many of them partially coated with a thin gypsum precipitate that is also found on sandstone inclusions in MOS and OS. This layer equates to Carter's Layer VI and marks the base of the 1992 excavation. Three radiocarbon determinations date RFS to 30.9-28.5 kya.

Figure S4. Site photographs of Mitchell 1992 and Stewart/Dewar 2009–15 (AMEMSA) excavations at Sehonghong. **a)** Excavation in process of Layer RFS (early MIS 2/late MIS 3). **b)** Section drawing of northern wall in progress near completion of 2009 AMEMSA season. **c)** Mitchell/Stewart/Dewar trench at completion of 2009 AMEMSA season (Carter 1971 trench located beneath spoil heap.

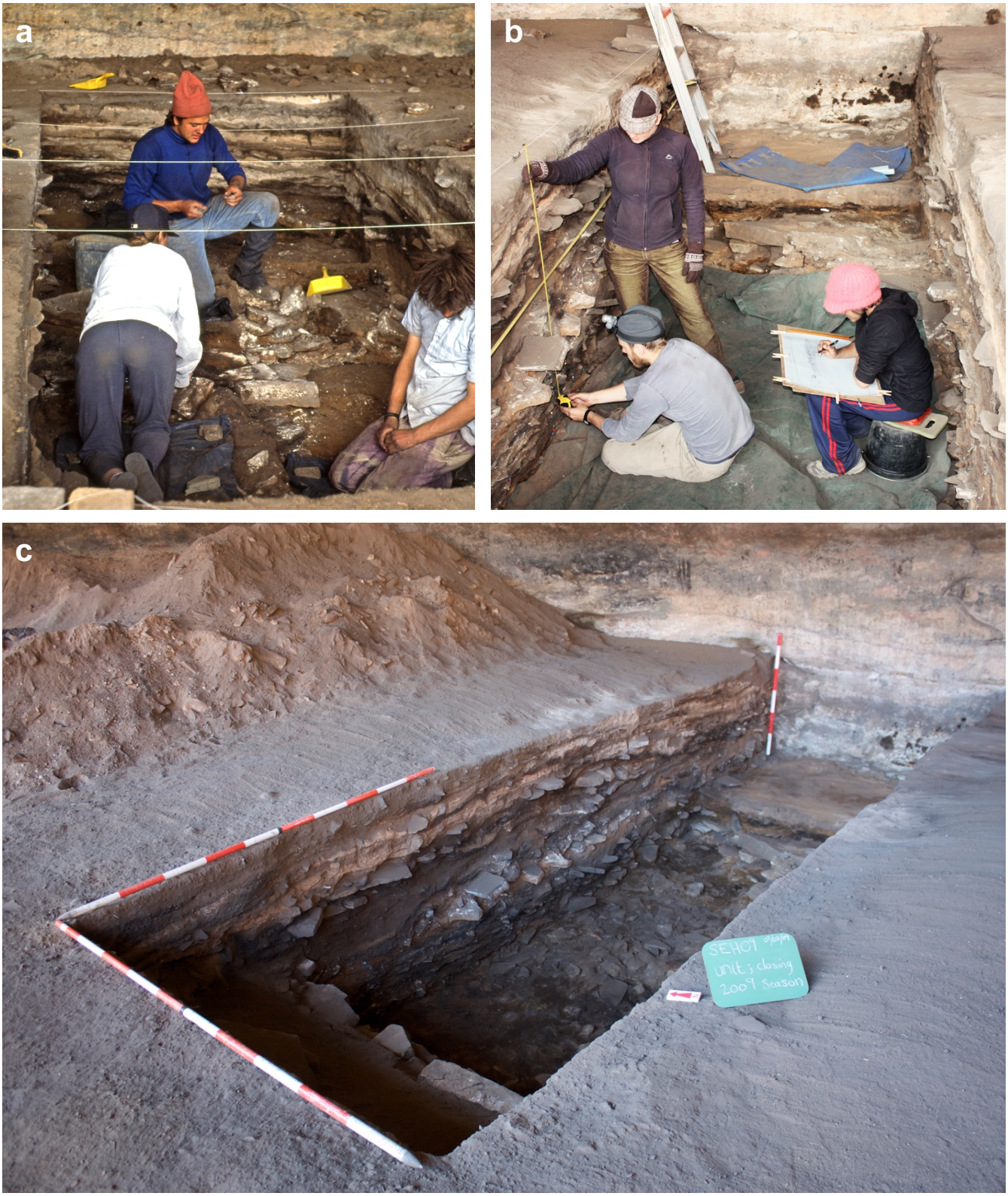

Table S3. Radiocarbon dates obtained from Mitchell and Stewart/Dewar excavations at Sehonghong Rock-Shelter.

Layer	Context	Laboratory number	14C BP	Cal. BP* (95.4 %)	Material	Reference
DC	011	Wk-34785	1132 ± 25	1057–933	Bone	Horsburgh et al.[34]
DC	011	Wk-34786	1132 ± 25	1057–933	Bone	Horsburgh et al.[34]
DC	011	Wk-34784	1201 ± 25	1173–974	Bone	Horsburgh et al.[34]
DC	017	Pta-6084	1240 ± 50	1265–980	Charcoal	Mitchell[32]
GAP	013	Pta-6063	1710 ± 20	1691–1528	Charcoal	Mitchell[32]
DC	011	Wk-34787	5870 ± 25	6736–6537	Bone	Horsburgh et al.[34]
GWA	001	Pta-6154	5950 ± 70	6931–6548	Charcoal	Mitchell[33]
ALP	006	Pta-6278	7290 ± 80	8297–7879	Charcoal	Mitchell[33]
ALP	014	Pta-6280	7090 ± 80	8007–7697	Charcoal	Mitchell[33]
ALP	022	Pta-6072	7210 ± 80	8173–7839	Charcoal	Mitchell[33]
ALP	117	Pta-6083	7010 ± 70	7942–7671	Charcoal	Mitchell[33]
SA	119	Pta-6368	9280 ± 45	10550–10255	Charcoal	Mitchell[33]
SA	062	Pta-6057	9740 ± 140	11595–10588	Charcoal	Mitchell[33]
BARF	064	Pta-6065	11090 ± 230	13395–12559	Charcoal	Mitchell[33]
RF	069	OxA-32926	12010 ± 50	14018–13773	Charcoal	Pargeter et al.[35]
RF	065	Pta-6282	12180 ± 110	14467–13731	Charcoal	Mitchell[31]
RF	065	OxA-32925	12355 ± 50	14712–14116	Charcoal	Pargeter et al.[35]
RF	065	OxA-32924	12420 ± 50	14877–14183	Charcoal	Pargeter et al.[35]
RF	090	Pta-6062	12410 ± 45	14735–14125	Charcoal	Mitchell[31]
RF	097	Pta-6058	12470 ± 100	15040–14137	Charcoal	Mitchell[31]
RBL/CLBRF	072	OxA-32923	12870 ± 55	15601–15163	Charcoal	Pargeter et al.[35]
RBL/CLBRF	072	OxA-32922	12690 ± 55	15725–15274	Charcoal	Pargeter et al.[35]
BAS	100	Pta-6060	15700 ± 150	19298–18600	Charcoal	Mitchell[31]
BAS	096A	Pta-6281	19400 ± 200	23853–22824	Charcoal	Mitchell[31]
BAS	126	Pta-6077	20200 ± 100	24495–23952	Charcoal	Mitchell[31]
BAS	126	OxA-32920	20270 ± 100	24648–24022	Charcoal	Pargeter et al.[35]
OS	127	OxA-32917	20100 ± 90	24420–23914	Charcoal	Pargeter et al.[35]
MOS	137	OxA-32919	20290 ± 90	24656–24058	Charcoal	Pargeter et al.[35]
MOS	137	OxA-32918	20460 ± 100	25019–24287	Charcoal	Pargeter et al.[35]
MOS	137	Pta-6059	20500 ± 230	25272–24061	Charcoal	Mitchell[30]
RFS	136	Pta-6271	25100 ± 300	29890–28466	Charcoal	Mitchell[30]
RFS	136	OxA-32915	25510 ± 150	30191–29206	Charcoal	Pargeter et al.[35]
RFS	136	OxA-32914	25870 ± 160	30615–26595	Charcoal	Pargeter et al.[35]
RFS	136	Pta-6268	26000 ± 430	30983–29243	Charcoal	Mitchell[30]
Unassigned	162	OxA-27689	25330 ± 130	29706–28692	Charcoal	Loftus et al.[28]
Unassigned	163	OxA-27690	28650 ± 200	33148–31867	Charcoal	Loftus et al.[28]
Unassigned	167	OxA-27691	29120 ± 190	33737–32804	Charcoal	Loftus et al.[28]
Unassigned	169	OxA-27692	29170 ± 190	33769–32858	Charcoal	Loftus et al.[28]
Unassigned	1030	OxA-27693	29200 ± 200	33801–32870	Charcoal	Loftus et al.[28]
Unassigned	1031	OxA-27694	28800 ± 190	33517–32197	Charcoal	Loftus et al.[28]
Unassigned	1036	OxA-27695	30910 ± 250	35332–34273	Charcoal	Loftus et al.[28]
Unassigned	1037	OxA-29696	31030 ± 250	35482–34417	Charcoal	Loftus et al.[28]
Unassigned	1111A	OxA-27696	30710 ± 240	35063–34127	Charcoal	Loftus et al.[28]

* Calibrated with OxCal v. 4.2[14] using the latest SHCal13 calibration curve for the Southern Hemisphere[15]

Figure S5. Section drawing of Sehonghong stratigraphic sequence – south wall of Mitchell/AMEMSA trench (modified after Mitchell[27], Fig. 2).

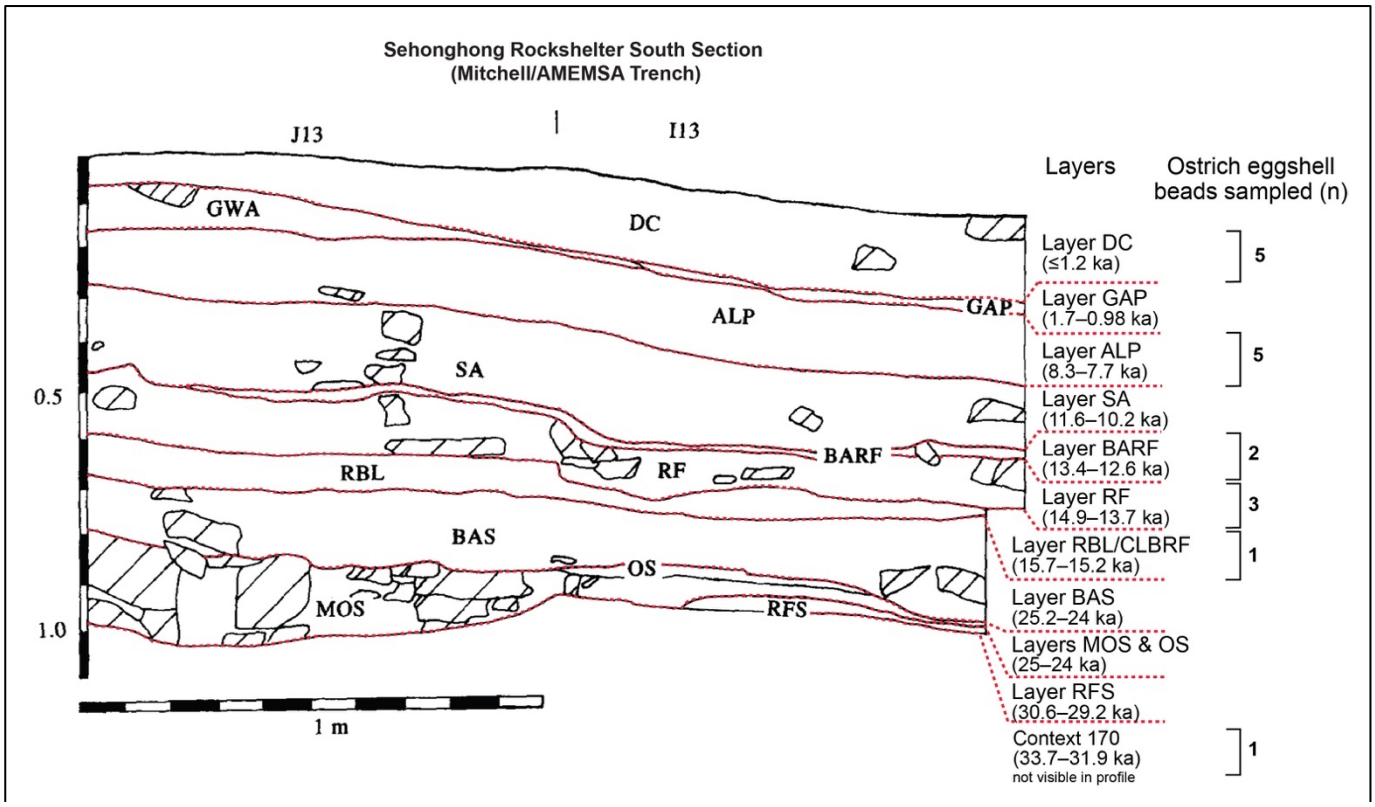

Figure S6. Photographs of ostrich eggshell beads sampled from Sehonghong

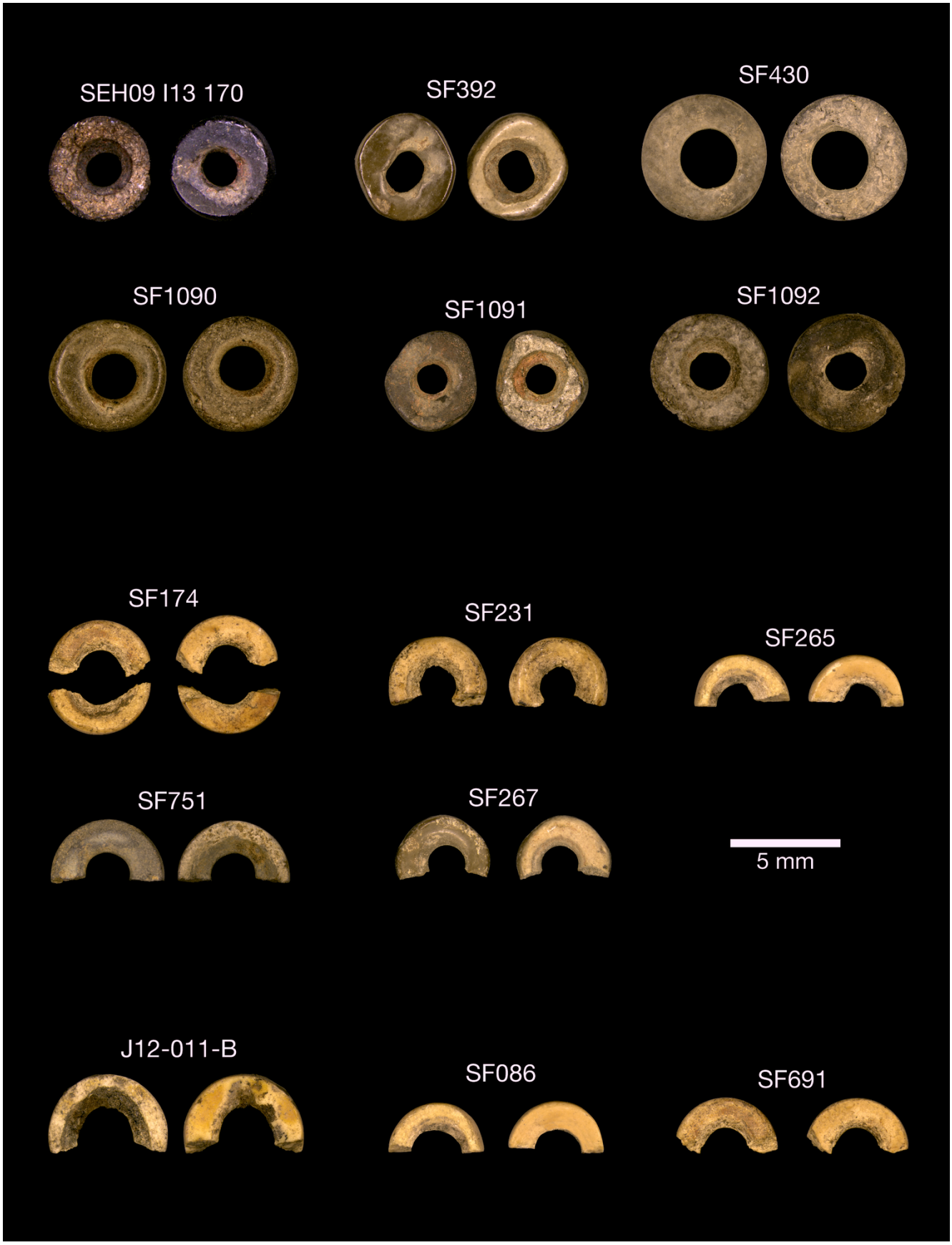

Table S4. Codes, details, and Sr isotopic compositions of samples employed to generate the highland baseline.

Sample code	Taxon	Locality/River	District/Province*	Lithology‡	87Sr/86Sr†	2SE ±	%2SE ±
			Soils extracts				
S1.1	-	Sehonghong	Thaba-Tseka	Dr, Cl	0.707969	0.000016	0.0023%
S7.1	-	Sehonghong	Thaba-Tseka	Dr	0.709800	0.000014	0.0019%
S14.1	-	Sehonghong	Thaba-Tseka	Dr, Cl	0.707729	0.000014	0.0020%
S15.1	-	Khomo-ea-Mollo	Thaba-Tseka	Cl	0.710071	0.000012	0.0017%
S17.1	-	Khomo-ea-Mollo	Thaba-Tseka	Cl	0.711644	0.000009	0.0013%
S19.1	-	Sehonghong	Thaba-Tseka	Dr	0.708752	0.000014	0.0019%
S26.1	-	Khomo-ea-Mollo	Thaba-Tseka	Cl	0.712386	0.000012	0.0017%
S28.1	-	Khomo-ea-Mollo	Thaba-Tseka	Cl	0.712696	0.000017	0.0024%
S31.1	-	Khomo-ea-Mollo	Thaba-Tseka	Cl	0.713272	0.000015	0.0021%
			Plants				
V107	*Themeda triandra*	Khomo-ea-Mollo	Thaba-Tseka	Cl	0.712404	0.000013	0.0018%
V108	*Themeda triandra*	Khomo-ea-Mollo	Thaba-Tseka	Cl	0.713681	0.000016	0.0022%
V109	*Themeda triandra*	Khomo-ea-Mollo	Thaba-Tseka	Cl	0.713089	0.000016	0.0022%
V110	*Themeda triandra*	Khomo-ea-Mollo	Thaba-Tseka	Cl	0.712713	0.000029	0.0041%
V144	*Themeda triandra*	Sehonghong	Thaba-Tseka	Dr	0.710648	0.000014	0.0020%
V145	*Themeda triandra*	Sehonghong	Thaba-Tseka	Dr	0.710105	0.000015	0.0021%
V146	*Themeda triandra*	Sehonghong	Thaba-Tseka	Dr	0.710024	0.000018	0.0025%
V148	*Themeda triandra*	Sehonghong	Thaba-Tseka	Dr	0.709536	0.000016	0.0023%
V151	*Themeda triandra*	Sehonghong	Thaba-Tseka	Dr	0.708713	0.000026	0.0037%
			Small mammals (tooth enamel)				
NMB6667	*Rhabdomys pumilio*	Sehlabathebe N.P.	Qacha's Nek	Cl	0.712061	0.000006	0.0009%
NMB6937	*Micaelamys namaquensis*	Mateanong	Mokhotlong	Dr	0.708523	0.000026	0.0037%
NMB7331	*Rhabdomys pumilio*	Marakabei	Maseru	Dr	0.708159	0.000008	0.0011%
NMB8166	*Otomys irroratus*	Bokong	Thaba-Tseka	Dr	0.711607	0.000009	0.0013%
NMB8202	*Micaelamys namaquensis*	Mount Moorosi	Quthing	Cl	0.715352	0.000011	0.0016%
NMB8357	*Otomys irroratus*	Oxbow Ski Lodge	Butha-Buthe	Dr	0.708785	0.000008	0.0011%
NMB8427	*Micaelamys namaquensis*	Moqotoane	Thaba-Tseka	Dr	0.707811	0.00001	0.0014%
NMB8641	*Micaelamys namaquensis*	Botsoela	Mafeteng	Dr	0.709177	0.000009	0.0013%
			Water (from de Villiers et al. 2000)				
U8	-	Orange-Senqu	Thaba-Tseka	Dr	0.70811	Unpublished	Unpublished
U7	-	Orange-Senqu	Thaba-Tseka	Dr	0.70824	"	"
U5	-	Orange-Senqu	Thaba-Tseka	Dr	0.70837	"	"
U4	-	Senqunyane	Maseru	Dr	0.70853	"	"
OV16(1)	-	Orange-Senqu	Mohale's Hoek	Dr, Cl, El	0.71232	"	"
OV16(2)	-	Orange-Senqu	Mohale's Hoek	Dr, Cl, El	0.7116	"	"
OV17	-	Orange-Senqu	Mohale's Hoek	Dr, Cl, El	0.70872	"	"
OV18	-	Orange-Senqu	Quthing	Dr, Cl, El	0.70904	"	"
OV19	-	Orange-Senqu	E. Cape (SA)	Dr, Cl, El	0.71229	"	"
OV9	-	Caledon	Butha-Buthe	Dt, Cl, El	0.70903	"	"
OV10	-	Caledon	Butha-Buthe	Dt, Cl, El	0.7091	"	"
OV12	-	Caledon	Leribe	Dt, Cl, El	0.7107	"	"
OV14	-	Caledon	Leribe	Dt, Cl, El	0.71171	"	"
OV15	-	Caledon	Berea	Dt, Cl, El	0.71141	"	"
OV11	-	Semena	Butha-Buthe	Dr, Cl	0.70887	"	"

* All in Lesotho exepct those specified 'SA' (South Africa).

‡ Lithology codes: Dr: Drakensberg Group; Dt: Intrusive dolerites; Cl: Clarens Formation; El: Elliot Formation; Mt: Molteno Formation.

† Mean value for the Sr standard NBS 987:

$^{87}Sr/^{86}Sr = 0.710250 \pm 0.000016$ (n = 16) Finnigan MAT 262.

$^{87}Sr/^{86}Sr = 0.710245 \pm 0.000014$ (n = 11) Thermo Scientific Triton Plus.

Accepted value of McArthur et al.[36] = 0.710248

Table S5. Codes, details, and Sr isotopic compositions of samples employed to generate working isoscape for the Karoo Supergroup (note: a single average value taken for replicates).

Sample code	Material	Taxon	Locality, Farm or River	District/ Province	Country	87Sr/86Sr*	2SE ±	%2SE ±
Drakensberg Group								
NMB6937	Enamel	*Micaelamys namaquensis*	Mateanong	Mokhotlong	Lesotho	0.708523	0.000026	0.0037%
NMB7331	Enamel	*Rhabdomys pumilio*	Marakabei	Maseru	Lesotho	0.708159	0.000008	0.0011%
NMB8166	Enamel	*Otomys irroratus*	Bokong	Thaba-Tseka	Lesotho	0.711607	0.000009	0.0013%
NMB8357	Enamel	*Otomys irroratus*	Oxbow Ski Lodge	Butha-Buthe	Lesotho	0.708785	0.000008	0.0011%
NMB8427	Enamel	*Micaelamys namaquensis*	Moqotoane	Thaba-Tseka	Lesotho	0.707811	0.00001	0.0014%
NMB8641	Enamel	*Micaelamys namaquensis*	Botsoela	Mafeteng	Lesotho	0.709177	0.000009	0.0013%
S7.1	Soil	-	Sehonghong	Thaba-Tseka	Lesotho	0.709800	0.000014	0.0019%
S19.1	Soil	-	Sehonghong	Thaba-Tseka	Lesotho	0.708752	0.000014	0.0019%
V144	Plant	*Themeda triandra*	Sehonghong	Thaba-Tseka	Lesotho	0.710648	0.000014	0.0020%
V145	Plant	*Themeda triandra*	Sehonghong	Thaba-Tseka	Lesotho	0.710105	0.000015	0.0021%
V146	Plant	*Themeda triandra*	Sehonghong	Thaba-Tseka	Lesotho	0.710024	0.000018	0.0025%
V148	Plant	*Themeda triandra*	Sehonghong	Thaba-Tseka	Lesotho	0.709536	0.000016	0.0023%
V151	Plant	*Themeda triandra*	Sehonghong	Thaba-Tseka	Lesotho	0.708713	0.000026	0.0037%
U4‡	Water	-	Senqunyane R.	Maseru	Lesotho	0.708530	unpublished	unpublished
U5‡	Water	-	Orange-Senqu R.	Thaba-Tseka	Lesotho	0.708370	unpublished	unpublished
U7‡	Water	-	Orange-Senqu R.	Thaba-Tseka	Lesotho	0.708240	unpublished	unpublished
U8‡	Water	-	Orange-Senqu R.	Thaba-Tseka	Lesotho	0.708110	unpublished	unpublished
Upper Stormberg Group (Clarens Formation)								
NMB6667	Enamel	*Rhabdomys pumilio*	Sehlabathebe N.P.	Qacha's Nek	Lesotho	0.712061	0.000006	0.0009%
S15.1	Soil	-	Khomo-ea-Mollo	Thaba-Tseka	Lesotho	0.710071	0.000012	0.0017%
S17.1	Soil	-	Khomo-ea-Mollo	Thaba-Tseka	Lesotho	0.711644	0.000009	0.0013%
S26.1	Soil	-	Khomo-ea-Mollo	Thaba-Tseka	Lesotho	0.712386	0.000012	0.0017%
S28.1	Soil	-	Khomo-ea-Mollo	Thaba-Tseka	Lesotho	0.712696	0.000017	0.0024%
S31.1	Soil	-	Khomo-ea-Mollo	Thaba-Tseka	Lesotho	0.713272	0.000015	0.0021%
V107	Plant	*Themeda triandra*	Khomo-ea-Mollo	Thaba-Tseka	Lesotho	0.712404	0.000013	0.0018%
V108	Plant	*Themeda triandra*	Khomo-ea-Mollo	Thaba-Tseka	Lesotho	0.713681	0.000016	0.0022%
V109	Plant	*Themeda triandra*	Khomo-ea-Mollo	Thaba-Tseka	Lesotho	0.713089	0.000016	0.0022%
V110	Plant	*Themeda triandra*	Khomo-ea-Mollo	Thaba-Tseka	Lesotho	0.712713	0.000029	0.0041%
Lower Stormberg Group (Elliot & Molteno Formations)								
NMB1674	Enamel	*Lepus saxatilis*	Nova	Free State	South Africa	0.713822	0.000008	0.0011%
NMB1781	Enamel	*Procavia capensis*	Northend	Free State	South Africa	0.712751	0.000007	0.0009%
NMB3448	Enamel	*Lepus saxatilis*	Malutizight	Free State	South Africa	0.712727	0.000009	0.0012%
NMB4054	Enamel	*Pedetes capensis*	Alpha	Free State	South Africa	0.712316	0.000008	0.0012%
NMB4131	Enamel	*Lepus saxatilis*	Letsoana Stad	Free State	South Africa	0.712660	0.000009	0.0013%
NMB4714	Enamel	*Procavia capensis*	Buffelsfontein	E. Cape	South Africa	0.715998	0.000006	0.0008%
NMB4858	Enamel	*Lepus saxatilis*	Ben Becula	E. Cape	South Africa	0.714393	0.000021	0.0030%
NMB7003	Enamel	*Gerbilliscus brantsii*	Maidenshope	Free State	South Africa	0.715171	0.00001	0.0014%
NMB8202	Enamel	*Micaelamys namaquensis*	Mount Moorosi	Quthing	Lesotho	0.715352	0.000011	0.0016%
NMB9196	Enamel	*Lepus saxatilis*	Qwa-Qwa N.P.	Free State	South Africa	0.714299	0.000013	0.0018%
OV25‡	Water	-	Caledon R.	Free State	South Africa	0.712650	unpublished	unpublished
Beaufort Group								
MMK3432	Enamel	*Pedetes capensis*	Doornkloof	N. Cape	South Africa	0.713774	0.000017	0.0024%
NMB2608	Enamel	*Pedetes capensis*	De Berg	Free State	South Africa	0.711978	0.000008	0.0011%
NMB2886	Enamel	*Pedetes capensis*	Kommetjiesfontein	Free State	South Africa	0.713259	0.000009	0.0013%
NMB3107	Enamel	*Lepus saxatilis*	Mooihoek	Free State	South Africa	0.714221	0.000007	0.0010%
NMB3126	Enamel	*Lepus saxatilis*	Asem	Free State	South Africa	0.714943	0.000012	0.0017%
NMB3263	Enamel	*Xerus inauris*	Graspan	Free State	South Africa	0.714677	0.000011	0.0015%
NMB3273	Enamel	*Pedetes capensis*	Eureka	Free State	South Africa	0.713577	0.000006	0.0008%
NMB3518	Enamel	*Procavia capensis*	Toledo	Free State	South Africa	0.716231	0.000009	0.0013%
NMB3705	Enamel	*Lepus saxatilis*	Allemansdrift	Free State	South Africa	0.712315	0.000011	0.0015%
NMB3739	Enamel	*Xerus inauris*	Eendrag	Free State	South Africa	0.713935	0.000007	0.0009%
NMB4333	Enamel	*Procavia capensis*	Brandlaagte	E. Cape	South Africa	0.715093	0.000007	0.0010%
OV27‡	Water	-	Orange-Senqu R.	Free State	South Africa	0.712300	unpublished	unpublished
OV27 (rep.)‡	Water	-	Orange-Senqu R.	Free State	South Africa	0.712160	unpublished	unpublished
Ecca/Dwyka Group								
MMK3158	Enamel	*Pronolagus rupestris*	Preezfontein	Free State	South Africa	0.712595	0.000012	0.0017%
MMK3411	Enamel	*Pedetes capensis*	Waterford	N. Cape	South Africa	0.716794	0.000016	0.0023%
MMK3164	Enamel	*Pronolagus rupestris*	Vogelfontein	N. Cape	South Africa	0.715665	0.000016	0.0022%
MMK322	Enamel	*Cryptomys hottentotus*	Benfontein	Free State	South Africa	0.715128	0.000013	0.0018%
MMK3466	Enamel	*Xerus inauris*	Uitkrans	N. Cape	South Africa	0.717322	0.000016	0.0022%
MMK3459	Enamel	*Xerus inauris*	Rodeseput	N. Cape	South Africa	0.715762	0.000018	0.0025%
MMK3551	Enamel	*Otomys unisulcatus*	Onder-Downes	N. Cape	South Africa	0.713224	0.000018	0.0025%
NMB1434	Enamel	*Lepus saxatilis*	La Riviera	Free State	South Africa	0.713940	0.000008	0.0011%
NMB1576	Enamel	*Xerus inauris*	Nielsview	Free State	South Africa	0.716169	0.000009	0.0012%
NMB3862	Enamel	*Lepus saxatilis*	Alma (Glen Alphen)	Free State	South Africa	0.715514	0.000007	0.0009%
OV30‡	Water	-	Orange-Senqu R.	N. Cape	South Africa	0.712860	unpublished	unpublished
OV30 (rep.)‡	Water	-	Orange-Senqu R.	N. Cape	South Africa	0.712540	unpublished	unpublished

* Mean value for the Sr standard NBS 987:
$^{87}Sr/^{86}Sr = 0.710250 \pm 0.000016$ (n = 16) Finnigan MAT 262.
$^{87}Sr/^{86}Sr = 0.710245 \pm 0.000014$ (n = 11) Thermo Scientific Triton Plus.
Accepted value of McArthur et al.[36] = 0.710248

‡ Values from de Villiers et al.[37]

Table S6. Ostrich eggshell bead Ca and Sr concentrations by ICP-OES.

Sample code	Site	Layer	Age (kcal BP)	Stage	Sr (ug/g)	Ca (ug/g)	Ca/Sr (wt.)	Ca (wt.%)
SF-4	Melikane	1	0.3–0.15	Late Holocene	35.6	200000	5610.2	20
SF-10	Melikane	2	3.3–0.15	Late Holocene	120.5	200000	1659.6	20
SF-13	Melikane	2	3.3–0.15	Late Holocene	81.2	200000	2461.7	20
SF-20	Melikane	2	3.3–0.15	Late Holocene	108.9	200000	1836.6	20
SF-29	Melikane	2	3.3–0.15	Late Holocene	116.3	200000	1719.4	20
SF-43	Melikane	2	3.3–0.15	Late Holocene	151.9	200000	1316.9	20
SF-48	Melikane	2	3.3–0.15	Late Holocene	73.6	200000	2719.1	20
SF-56	Melikane	2	3.3–0.15	Late Holocene	148.9	200000	1342.9	20
SF-70	Melikane	2	3.3–0.15	Late Holocene	78.6	200000	2543.1	20
SF-87	Melikane	2	3.3–0.15	Late Holocene	47.4	200000	4217.7	20
SF-90	Melikane	2	3.3–0.15	Late Holocene	125.5	200000	1594.3	20
SF-86	Sehonghong	DC	1.26–0.98	Late Holocene	116.8	190645	1632.6	19.06
SF-101	Sehonghong	DC	1.26–0.98	Late Holocene	158.5	193538	1221.1	19.35
J12-11B	Sehonghong	DC	1.26–0.98	Late Holocene	132	194545	1473.3	19.45
J12-11C	Sehonghong	DC	1.26–0.98	Late Holocene	160.3	205795	1283.8	20.58
SF-691	Sehonghong	DC	1.26–0.98	Late Holocene	51.2	194569	2339.1	19.46
SF-174	Sehonghong	ALP	8.3–7.67	Early Holocene	177.1	196739	1110.8	19.67
SF-231	Sehonghong	ALP	8.3–7.67	Early Holocene	91.5	199125	2176.2	19.91
SF-265	Sehonghong	ALP	8.3–7.67	Early Holocene	87.8	191000	2175.9	19.1
SF-267	Sehonghong	ALP	8.3–7.67	Early Holocene	56.2	205776	3658.8	20.58
SF-751	Sehonghong	ALP	8.3–7.67	Early Holocene	85.9	201016	3799.7	20.1
SF-430	Sehonghong	BARF	13.4–12.6	Late Pleistocene	83.3	194728	2337.2	19.47
SF-1090	Sehonghong	RF	15–13.7	Late Pleistocene	67.1	202838	3024.4	20.28
SF-1091	Sehonghong	RF	15–13.7	Late Pleistocene	79.2	212600	2683.7	21.26
SF-1092	Sehonghong	RF	15–13.7	Late Pleistocene	139.4	193963	1391.5	19.4
SF-392	Sehonghong	RBL-CRBLF	15.7–15.2	Late Pleistocene	85.9	155924	1814.7	15.59
I13-170	Sehonghong	n/a	33.7–31.9	Late Pleistocene	Unobtained	Unobtained	Unobtained	Unobtained

Table S7. Soil, plant and small mammal tooth enamel Ca and Sr concentrations by ICP-OES.

Sample code	Taxon	Locality/Farm	Province/ District	Country	Lithology*	Sr (ug/g)	Ca (ug/g)	Ca/Sr (wt.)	Ca (wt. %)
				Soils					
S1.1 (HNO3)	-	Sehonghong	Thaba-Tseka	Lesotho	Dr, Cl	8.4	3186	377.5	0.32
S1.1 (NH4Cl)	-	Sehonghong	Thaba-Tseka	Lesotho	Dr, Cl	9.5	4434	465	0.44
S7.1 (HNO3)	-	Sehonghong	Thaba-Tseka	Lesotho	Dr	3.6	1394.8	387	0.14
S7.1 (NH4Cl)	-	Sehonghong	Thaba-Tseka	Lesotho	Dr	9.7	2726	280.5	0.27
S14.1 (HNO3)	-	Sehonghong	Thaba-Tseka	Lesotho	Dr, Cl	10	4252	425	0.43
S14.1 (NH4Cl)	-	Sehonghong	Thaba-Tseka	Lesotho	Dr, Cl	10.1	4136	409.7	0.41
S15.1 (HNO3)	-	Khomo-ea-Mollo	Thaba-Tseka	Lesotho	Cl	Unobtained	Unobtained	Unobtained	Unobtained
S15.1 (NH4Cl)	-	Khomo-ea-Mollo	Thaba-Tseka	Lesotho	Cl	Unobtained	Unobtained	Unobtained	Unobtained
S17.1 (HNO3)	-	Khomo-ea-Mollo	Thaba-Tseka	Lesotho	Cl	7.6	3112	407.1	0.31
S17.1 (NH4Cl)	-	Khomo-ea-Mollo	Thaba-Tseka	Lesotho	Cl	9.3	3038	327.3	0.3
S19.1 (HNO3)	-	Sehonghong	Thaba-Tseka	Lesotho	Dr	9.7	3544	364.8	0.35
S19.1 (NH4Cl)	-	Sehonghong	Thaba-Tseka	Lesotho	Dr	11.4	2874	253	0.29
S26.1 (HNO3)	-	Khomo-ea-Mollo	Thaba-Tseka	Lesotho	Cl	13	4656	357.8	0.47
S26.1 (NH4Cl)	-	Khomo-ea-Mollo	Thaba-Tseka	Lesotho	Cl	7.9	3182	404.8	0.32
S28.1 (HNO3)	-	Khomo-ea-Mollo	Thaba-Tseka	Lesotho	Cl	Unobtained	Unobtained	Unobtained	Unobtained
S28.1 (NH4Cl)	-	Khomo-ea-Mollo	Thaba-Tseka	Lesotho	Cl	Unobtained	Unobtained	Unobtained	Unobtained
S31.1 (HNO3)	-	Khomo-ea-Mollo	Thaba-Tseka	Lesotho	Cl	3.9	1188.2	301.6	0.12
S31.1 (NH4Cl)	-	Khomo-ea-Mollo	Thaba-Tseka	Lesotho	Cl	9.4	2760	293.5	0.28
				Plants					
V107	*Themeda triandra*	Khomo-ea-Mollo	Thaba-Tseka	Lesotho	Cl	20.9	8764.9	419.6	0.88
V108	*Themeda triandra*	Khomo-ea-Mollo	Thaba-Tseka	Lesotho	Cl	150.4	48481.3	322.3	4.85
V109	*Themeda triandra*	Khomo-ea-Mollo	Thaba-Tseka	Lesotho	Cl	17.3	2925.9	168.8	0.29
V110	*Themeda triandra*	Khomo-ea-Mollo	Thaba-Tseka	Lesotho	Cl	30.8	12422.3	403.9	1.24
V144	*Themeda triandra*	Sehonghong	Thaba-Tseka	Lesotho	Dr	11.3	3626.7	322.1	0.36
V145	*Themeda triandra*	Sehonghong	Thaba-Tseka	Lesotho	Dr	Unobtained	Unobtained	Unobtained	Unobtained
V146	*Themeda triandra*	Sehonghong	Thaba-Tseka	Lesotho	Dr	27.1	11802.7	435.5	1.18
V148	*Themeda triandra*	Sehonghong	Thaba-Tseka	Lesotho	Dr	11.2	5469.6	489.8	0.55
V151	*Themeda triandra*	Sehonghong	Thaba-Tseka	Lesotho	Dr	9.6	2344	245	0.23
				Small mammals (tooth enamel)					
MMK322	*Cryptomys hottentotus*	Benfontein	Free State	South Africa	E/D	343.3	225600	657.2	22.56
MMK3158	*Pronolagus rupestris*	Preezfontein	Free State	South Africa	E/D	480.4	240480	500.6	24.05
MMK3164	*Pronolagus rupestris*	Vogelfontein	N. Cape	South Africa	E/D	208.3	212240	1018.8	21.22
MMK3411	*Pedetes capensis*	Waterford	N. Cape	South Africa	E/D	232.6	315200	1355.3	31.52
MMK3432	*Pedetes capensis*	Doornkloof	N. Cape	South Africa	B	112.5	300240	2669.3	30.02
MMK3466	*Xerus inauris*	Uitkrans	N. Cape	South Africa	E/D	370.5	245440	662.5	24.54
MMK3459	*Xerus inauris*	Rodeseput	N. Cape	South Africa	E/D	249	250480	1006.1	25.05
MMK3551	*Otomys unisulcatus*	Onder-Downes	N. Cape	South Africa	E/D	353.8	276800	782.3	27.68
NMB1434	*Lepus saxatilis*	La Riviera	Free State	South Africa	E/D	110.4	172206	1559.3	17.22
NMB1576	*Xerus inauris*	Nielsview	Free State	South Africa	E/D	211.8	206170	973.4	20.62
NMB1674	*Lepus saxatilis*	Nova	Free State	South Africa	LS	309.3	290909	940.5	29.09
NMB1781	*Procavia capensis*	Northend	Free State	South Africa	LS	Unobtained	Unobtained	Unobtained	Unobtained
NMB2608	*Pedetes capensis*	De Berg	Free State	South Africa	B	303.9	378468	1245.5	37.85
NMB2886	*Pedetes capensis*	Kommetjiesfontein	Free State	South Africa	B	64.2	190657	2969.7	19.07
NMB3107	*Lepus saxatilis*	Mooihoek	Free State	South Africa	B	179.6	327872	1825.8	32.79
NMB3126	*Lepus saxatilis*	Asem	Free State	South Africa	B	275.2	278089	1010.7	27.81
NMB3263	*Xerus inauris*	Graspan	Free State	South Africa	B	76.1	207600	2728.5	20.76
NMB3273	*Pedetes capensis*	Eureka	Free State	South Africa	B	314.5	327130	1040	32.71
NMB3448	*Lepus saxatilis*	Malutizight	Free State	South Africa	LS	219.8	301373	1371.1	30.14
NMB3518	*Procavia capensis*	Toledo	Free State	South Africa	B	Unobtained	Unobtained	Unobtained	Unobtained
NMB3705	*Lepus saxatilis*	Allemansdrift	Free State	South Africa	B	158.2	258229	1632	25.82
NMB3739	*Xerus inauris*	Eendrag	Free State	South Africa	B	133.5	286563	2146.3	28.66
NMB3862	*Lepus saxatilis*	Alma (Glen Alphen)	Free State	South Africa	E/D	236	277212	1174.8	27.72
NMB4054	*Pedetes capensis*	Alpha	Free State	South Africa	LS	210.7	298696	1417.7	29.87
NMB4131	*Lepus saxatilis*	Letsoana Stad	Free State	South Africa	LS	129.7	244328	1883.3	24.43
NMB4333	*Procavia capensis*	Brandlaagte	E. Cape	South Africa	LS	Unobtained	Unobtained	Unobtained	Unobtained
NMB4714	*Procavia capensis*	Buffelsfontein	E. Cape	South Africa	LS	Unobtained	Unobtained	Unobtained	Unobtained
NMB4858	*Lepus saxatilis*	Ben Becula	E. Cape	South Africa	LS	203.7	297763	1461.9	29.78
NMB6667	*Rhabdomys pumilio*	Sehlabathebe N.P.	Qacha's Nek	Lesotho	Cl	557.2	413667	742.4	41.37
NMB6937	*Micaelamys namaquensis*	Mateanong	Mokhotlong	Lesotho	Dr	86.4	278629	3226	27.86
NMB7003	*Gerbilliscus brantsii*	Maidenshope	Free State	South Africa	LS	182.8	200727	1098.3	20.07
NMB7331	*Rhabdomys pumilio*	Marakabei	Maseru	Lesotho	Dr	104.8	345686	3298.4	34.57
NMB8166	*Otomys irroratus*	Bokong	Thaba-Tseka	Lesotho	Dr	104.8	165000	1574.7	16.5
NMB8202	*Micaelamys namaquensis*	Mount Moorosi	Quthing	Lesotho	Cl	223.9	327963	1464.8	32.8
NMB8357	*Otomys irroratus*	Oxbow Ski Lodge	Butha-Buthe	Lesotho	Dr	147.1	241642	1642.8	24.16
NMB8427	*Micaelamys namaquensis*	Moqotoane	Thaba-Tseka	Lesotho	Dr	94.4	278148	2945.1	27.81
NMB8641	*Micaelamys namaquensis*	Botsoela	Mafeteng	Lesotho	Dr	128.4	415614	3236.3	41.56
NMB9196	*Lepus saxatilis*	Qwa-Qwa N.P.	Free State	South Africa	LS	126.4	185684	1468.5	18.57

* Lithology codes: Dr: Drakensberg Group; Cl: Clarens Formation; LS: Lower Stormberg Group; B: Beaufort Group; E/D: Ecca/Dwyka Group.

Figure S7. Map of (a) small mammal tooth enamel and water and (b) plant and soil sample locations for generating both the highland baseline and the Karoo Supergroup working isoscape.

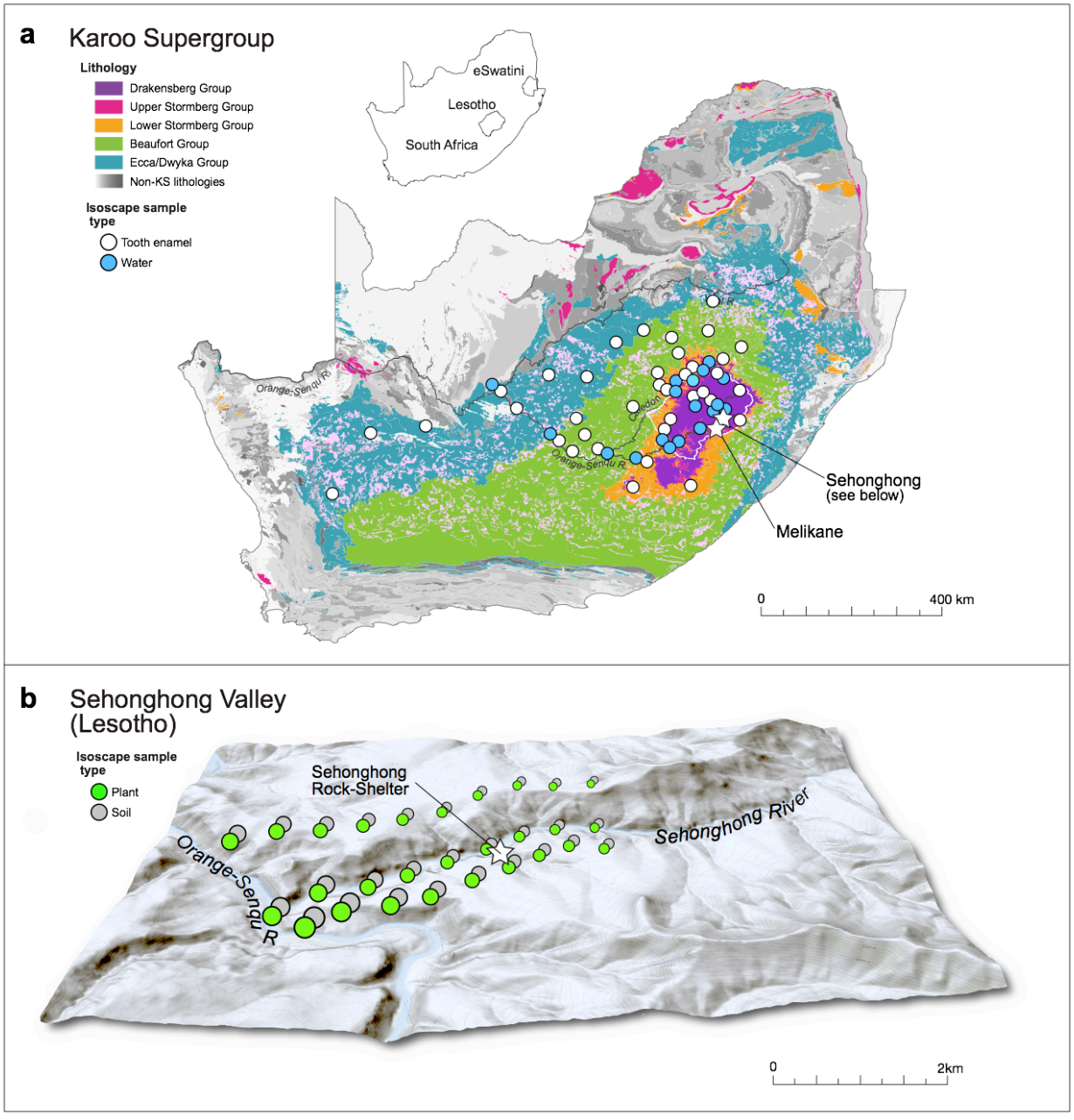

Table S8. Spatial coordinates of samples used to generate the Karoo Supergroup working isoscape.

Sample code	87Sr/86Sr	Y	X	Material	Comment
MMK3158	0.71260	-29.80000	25.38333	Enamel	
MMK3411	0.71679	-29.60000	24.08333	Enamel	
MMK3432	0.71377	-30.33333	25.03333	Enamel	
MMK3164	0.71567	-28.90000	23.65000	Enamel	
MMK322	0.71513	-28.83333	24.81667	Enamel	
MMK3466	0.71732	-29.95000	22.05000	Enamel	
MMK3459	0.71576	-30.16667	20.80000	Enamel	
MMK3551	0.71322	-31.51667	19.93333	Enamel	
NMB1434	0.71394	-28.07439	26.32528	Enamel	
NMB1576	0.71617	-28.87067	25.68567	Enamel	
NMB1674	0.71382	-29.03883	27.37003	Enamel	
NMB1781	0.71275	-28.85009	27.91170	Enamel	
NMB2608	0.71198	-29.57032	26.72394	Enamel	
NMB2886	0.71326	-30.19894	25.63301	Enamel	
NMB3107	0.71422	-28.20245	29.15450	Enamel	
NMB3126	0.71494	-28.33139	27.75125	Enamel	
NMB3263	0.71468	-27.81233	26.96788	Enamel	
NMB3273	0.71358	-27.98065	27.58900	Enamel	
NMB3448	0.71273	-28.73803	28.06398	Enamel	
NMB3518	0.71623	-27.83078	28.41297	Enamel	
NMB3705	0.71232	-30.54572	25.35370	Enamel	
NMB3739	0.71394	-30.52267	25.91769	Enamel	
NMB3862	0.71551	-27.12437	28.52160	Enamel	
NMB4054	0.71232	-29.11233	27.64440	Enamel	
NMB4131	0.71266	-28.57220	28.42074	Enamel	
NMB4333	0.71509	-30.80944	27.04312	Enamel	
NMB4714	0.71600	-31.36518	26.71571	Enamel	
NMB4858	0.71439	-31.34242	28.02520	Enamel	
NMB6667	0.71206	-29.86902	29.11613	Enamel	
NMB6937	0.70852	-29.20000	29.13000	Enamel	
NMB7003	0.71517	-28.78391	27.29614	Enamel	
NMB7331	0.70816	-29.32000	28.08000	Enamel	
NMB8166	0.71161	-29.22000	28.32000	Enamel	
NMB8202	0.71535	-30.14000	27.53000	Enamel	
NMB8357	0.70879	-28.47000	28.41000	Enamel	
NMB8427	0.70781	-29.42000	28.48000	Enamel	
NMB8641	0.70918	-29.84858	27.55989	Enamel	
NMB9196	0.71430	-28.46383	28.70372	Enamel	
U8‡	0.70811	-29.60000	28.63000	Water	
U7‡	0.70824	-29.53000	28.583	Water	
U5‡	0.70837	-29.60000	28.6833	Water	
U4‡	0.70853	-29.56660	28.1333	Water	
OV16‡	0.71196	-30.31666	27.4	Water	Mean of OV16 1 & 2
OV17‡	0.70872	-30.03330	28.23333	Water	
OV18‡	0.70904	-30.36667	27.73333	Water	
OV19‡	0.71229	-30.45000	27.56666	Water	
OV9‡	0.70903	-28.63333	28.41666	Water	
OV10‡	0.70910	-28.70000	28.36666	Water	
OV12‡	0.71070	-28.90000	28.03333	Water	
OV14‡	0.71171	-29.08333	27.66666	Water	
OV15‡	0.71141	-29.11666	27.65	Water	
OV11‡	0.70887	-28.76667	28.65	Water	
OV20‡	0.71067	-30.73333	26.78333	Water	Mean of OV20 1 & 2

‡ Values from de Villiers et al.[37]

3. Further details on materials and methods

3.1 Sample preparation

Interior portions of ostrich eggshell beads were drilled using a sterilized dental micro-drill device to extract sufficient and unaltered material for Sr isotopic analysis. This was precisely weighed and approximately 5 mg of powdered bead material was transferred into an acid-washed 15 ml teflon beaker. All sample digestions were carried out in a HEPA-filtered fume hood in acid-washed labware. Acids were double-distilled Seastar-grade and water was deionized. Up to 2 ml of HNO_3 was used to digest the bead powders. Once the reaction was complete, 100 microliters of H_2O_2 was added by pipette and the sample beaker was capped tightly. Samples were heated overnight at 100° C, followed by evaporation to dryness at 80°C. Following additional treatment with HNO_3 the sample was dried at 100°C, taken up in 1ml HNO_3 and diluted to 5 ml with H_2O for a final acid concentration of 20% HNO_3. This solution was transferred to a low-density polyethylene (LDP) bottle prior to analysis.

Plant samples were freeze-dried and crushed using an acid--cleaned agate mortar and pestle, prior to high pressure microwave acid digestion. Approximately 500 mg of finely ground material was weighed into acid-cleaned microwave vessels and digested using high-pressure hydrothermal microwave acid digestion (CEM MARS 5) in a concentrated HNO_3-HCl acid mixture at 240°C and 350psi. The digest solution was further treated in several steps in Savillex Teflon beakers. Several HNO_3-H_2O_2 additions followed by evaporation were employed until all residues and organics were gone. Clear acid solutions were then diluted to 5% HNO_3 and transferred (10 ml total) into 15ml LDP bottles.

Soil samples were freeze-dried and crushed using an acid-cleaned agate mortar and pestle, prior to sequential extraction steps for isolating (1) loosely bound soil cations (plant-available pool), and (2) the non-silicate mineral nutrient pool (mainly carbonate and phosphate) in the soils. Approximately 500 mg of finely ground soil material was weighed and transferred into polycarbonate 15 ml centrifuge tubes, then subjected to the 2-step sequential extraction procedure as follows:

1) Overnight agitation on a shaker table at room temperature in 5ml of pH neutral 1M ammonium chloride (NH_4Cl), followed by centrifugation, transfer of the leachate to a 15ml LDP bottle, rinsing of the residue with 5 ml H_2O, followed by centrifugation and transfer of the rinse solution for a combined NH_4Cl leach solution total of 10 ml.
2) Overnight agitation of residue on a shaker table at room temperature with 5ml of 1M HNO_3 for extraction of the non-silicate mineral cation fraction, resulting (using same procedure as above) in a combined solution total of 10 ml.

Prior to analysis, these 10 ml soil leach solutions were filtered at 0.45 microns, and an aliquot was extracted for further treatment in several steps using HNO_3 and H_2O_2 in Teflon beakers (as above).

Individual small mammal teeth were pre-cleaned following the reductive-oxidative cleaning protocols detailed in Gleason et al.[38] to decontaminate surfaces of all soil or otherwise adhering contaminant Sr, slightly modified for this study. Briefly, each individual small mammal tooth was weighed and then subjected to a multi-step oxidative-reductive cleaning procedure involving several reagents plus heat and ultra-sonification in the following order:

1) Sodium citrate, sodium bicarbonate and sodium dithionite (CBD) reductive cleaning;
2) Sodium hydroxide (NaOH) treatment to remove any opaline contaminants;
3) Hydrogen peroxide oxidative cleaning to destroy any remaining organics;
4) Glacial acetic acid to assist with removal of carbonate.

Following the oxidative-reductive cleaning procedure, mammal teeth were individually weighed (~0.05 grams each) and rinsed in 0.05N HNO_3 followed by multiple rinses in H_2O, then digested in 2ml of HNO_3. Following centrifugation, 1ml of supernatant was removed and transferred to a 15 ml teflon beaker for further hotplate pre-treatment with hydrogen peroxide to break down remaining organics following the same procedures applied to the soil and vegetation samples (as detailed above). This aliquot was diluted to a volume of 5 ml 20% HNO_3 (as above) and transferred to a LDP bottle prior to analysis.

3.2 Sr Isotopic Analysis by Thermal Ionization Mass Spectrometry (TIMS)

Prior to Sr isotopic analysis, a proportion of each digest solution equivalent to ~100 ng of Sr was transferred into a clean 15 ml teflon beaker and dried down in a HEPA-filtered fume hood. The residue was then taken up in 1ml of 3N Seastar HNO_3, capped and set aside for Sr ion exchange column chemistry. Samples were loaded in 3N Seastar HNO_3 onto miniaturized Sr-spec resin (Eichrom) chromatographic columns for separation of Sr from matrix[38,39]. High-precision Sr isotope ratios were determined at the University of Michigan on a Finnigan MAT 262 solid source thermal ionization mass spectrometer (TIMS) equipped with 8 Faraday detectors, or a Triton Plus (Thermo Scientific) TIMS instrument equipped with 8 Faraday collectors employed in static mode configuration. Sr was loaded either on tungsten (W) filaments using 1N HCl with phosphoric acid binder and tantalum oxide activator, or on rhenium (Re) filaments in 7N HNO_3 with tantalum fluoride activator, dried down and loaded on a sample turret with the NBS 987 Sr isotope standard[39]. All data were collected in static mode using a ~2.0V ^{88}Sr beam, with average analytical precision of ±0.0019% (2SE) on the $^{87}Sr/^{86}Sr$ ratio (n = 150 ratios on the Finnigan MAT 262; n = 400 ratios on the Triton Plus). ^{85}Rb was monitored to correct for ^{87}Rb mass interference (< 0.1 mV) on ^{87}Sr. $^{87}Sr/^{86}Sr$ ratios were normalized to $^{86}Sr/^{88}Sr$ =0.1194 to correct for instrumental mass bias using (online) exponential law algorithms, and standard online statistical corrections for collector gain efficiencies and isotope ratio outlier analysis employed. The mean value for the Sr standard NBS 987 over the course of this study was $^{87}Sr/^{86}Sr = 0.710250 \pm 0.000016$ (n = 16) for the Finnigan MAT 262, and $^{87}Sr/^{86}Sr = 0.710245 \pm 0.000014$ (n = 11) for the Triton Plus. The accepted value from McArthur et al.[36] is 0.710248; therefore, no corrections were required to adjust $^{87}Sr/^{86}Sr$ ratios. Total process Sr blanks were ~ 50 pg, equivalent to < 1/1000 of the sample processed, requiring no blank corrections to the data.

3.3. Inductively Coupled Plasma Optical Emission Spectrometry (ICP-OES) Analysis

ICP-OES cation elemental analysis was conducted at the University of Michigan on a Perkin-Elmer Optima 3300DV ICP-OES. All sample solutions and calibration standards were run using 2% Trace Metal grade HNO_3. Ca and Sr abundances, and Ca/Sr elemental ratios, are accurate in most cases to better than ± 5% based on repeat analysis of replicates, reference materials (TMDW run at different concentrations), bracketing (calibration check) standards, and system blanks for quantifying limits of detection.

4. Statistical methods and results

All statistical analyses were conducted using RStudio software[40]. An alpha level of 0.05 was employed as the significance threshold.

The relevant $^{87}Sr/^{86}Sr$ values were distributed into the following groups:

- 'bead' (combined sample of ostrich eggshell beads from Melikane and Sehonghong)
- 'highland' (multi-proxy highland baseline);
- 'draken' (Drakensberg Group)
- 'upstorm' (Upper Stormberg Group)
- 'lowstorm' (Lower Stormberg Group)
- 'beaufort' (Beaufort Group)
- 'eccadwyka' (Ecca/Dwyka Groups)

Prior to conducting the *t*-tests, Shapiro-Wilk tests and F-tests were employed to assess assumptions of distribution normality and sample variance equality, respectively. One extreme outlier (0.75554) in the 'bead' group was excluded from these analyses (as well as from the subsequent *t*-tests). Results of the Shapiro-Wilk tests show that all groups are normally distributed except 'highland'. This group, however, has a large enough sample size (n = 40) that we can safely assume the data structure is close to normal. Results of the F-tests, run between the 'bead' group and each of the other groups, show that variance is statistically equal in all cases except between 'bead' and 'draken'. With all assumptions verified, we employed Welch's *t*-tests between the 'beads' group and all others due to differences in variance ('bead' vs. 'draken') and sample sizes ('bead' vs. each of the other groups). Below is the R code that we inputted into RStudio and the outputs containing all exact values.

R code

```
srplot=read.csv(file.choose(), header=TRUE)
attach(srplot)
srplot
bead=subset(Sr,sample=='bead')
highland=subset(Sr,sample=='highland')
draken=subset(Sr,sample=='draken')
upstorm=subset(Sr,sample=='upstorm')
lowstorm=subset(Sr,sample=='lowstorm')
beaufort=subset(Sr,sample=='beaufort')
eccadwya=subset(Sr,sample=='eccadwya')
```

Shapiro-Wilk tests

```
> shapiro.test(bead)
        Shapiro-Wilk normality test
data:  bead
W = 0.94673, p-value = 0.1943

> shapiro.test(highland)
        Shapiro-Wilk normality test
data:  highland
W = 0.9145, p-value = 0.005191
```

```
> shapiro.test(draken)
        Shapiro-Wilk normality test
data:  draken
W = 0.9125, p-value = 0.1102

> shapiro.test(upstorm)
        Shapiro-Wilk normality test
data:  upstorm
W = 0.90356, p-value = 0.2396

> shapiro.test(lowstorm)
        Shapiro-Wilk normality test
data:  lowstorm
W = 0.95239, p-value = 0.6722

> shapiro.test(beaufort)
        Shapiro-Wilk normality test
data:  beaufort
W = 0.96552, p-value = 0.8588

> shapiro.test(eccadwya)
        Shapiro-Wilk normality test
data:  eccadwya
W = 0.92706, p-value = 0.3818
```

F-tests

```
> var.test(bead,highland)
        F test to compare two variances
data:  bead and highland
F = 0.97023, num df = 25, denom df = 39, p-value = 0.9553
alternative hypothesis: true ratio of variances is not equal to 1
95 percent confidence interval:
 0.4841102 2.0600388
sample estimates:
ratio of variances
         0.9702321

> var.test(bead,draken)
        F test to compare two variances
data:  bead and draken
F = 3.0009, num df = 25, denom df = 16, p-value = 0.02604
alternative hypothesis: true ratio of variances is not equal to 1
95 percent confidence interval:
 1.148095 7.154237
sample estimates:
ratio of variances
          3.000936

> var.test(bead,upstorm)
        F test to compare two variances
data:  bead and upstorm
F = 3.1389, num df = 25, denom df = 9, p-value = 0.07781
alternative hypothesis: true ratio of variances is not equal to 1
95 percent confidence interval:
 0.8710724 8.4017992
```

```
sample estimates:
ratio of variances
         3.138933

> var.test(bead,lowstorm)
            F test to compare two variances
data:  bead and lowstorm
F = 1.3579, num df = 25, denom df = 11, p-value = 0.6101
alternative hypothesis: true ratio of variances is not equal to 1
95 percent confidence interval:
 0.4294846 3.4765789
sample estimates:
ratio of variances
         1.357877

> var.test(bead,beaufort)
            F test to compare two variances
data:  bead and beaufort
F = 1.9386, num df = 25, denom df = 11, p-value = 0.2512
alternative hypothesis: true ratio of variances is not equal to 1
95 percent confidence interval:
 0.6131691 4.9634622
sample estimates:
ratio of variances
         1.938622

> var.test(bead,eccadwya)
            F test to compare two variances
data:  bead and eccadwya
F = 1.2014, num df = 25, denom df = 10, p-value = 0.7945
alternative hypothesis: true ratio of variances is not equal to 1
95 percent confidence interval:
 0.3581276 3.1397484
sample estimates:
ratio of variances
         1.201373
```

Welch's *t*-tests

```
> t.test(bead,highland)
            Welch Two Sample t-test
data:  bead and highland
t = 10.673, df = 54.141, p-value = 6.269e-15
alternative hypothesis: true difference in means is not equal to 0
95 percent confidence interval:
 0.003929306 0.005746791
sample estimates:
mean of x mean of y
0.7150729 0.7102349

> t.test(bead,draken)
            Welch Two Sample t-test
data:  bead and draken
t = 13.833, df = 40.528, p-value < 2.2e-16
alternative hypothesis: true difference in means is not equal to 0
95 percent confidence interval:
```

0.005091041 0.006832452
sample estimates:
mean of x mean of y
0.7150729 0.7091112

> t.test(bead,upstorm)
Welch Two Sample t-test
data: bead and upstorm
t = 5.6319, df = 28.759, p-value = 4.517e-06
alternative hypothesis: true difference in means is not equal to 0
95 percent confidence interval:
0.001700819 0.003641627
sample estimates:
mean of x mean of y
0.7150729 0.7124017

> t.test(bead,lowstorm)
Welch Two Sample t-test
data: bead and lowstorm
t = 2.6633, df = 24.819, p-value = 0.01339
alternative hypothesis: true difference in means is not equal to 0
95 percent confidence interval:
0.0003407506 0.0026694288
sample estimates:
mean of x mean of y
0.7150729 0.7135678

> t.test(bead,beaufort)
Welch Two Sample t-test
data: bead and beaufort
t = 2.3904, df = 29.204, p-value = 0.0235
alternative hypothesis: true difference in means is not equal to 0
95 percent confidence interval:
0.0001765024 0.0022638438
sample estimates:
mean of x mean of y
0.7150729 0.7138528

> t.test(bead,eccadwya)
Welch Two Sample t-test
data: bead and eccadwya
t = 0.14882, df = 20.618, p-value = 0.8831
alternative hypothesis: true difference in means is not equal to 0
95 percent confidence interval:
-0.001168109 0.001347955
sample estimates:
mean of x mean of y
0.7150729 0.7149830

5. Methods used to produce Figs. 1a and 6a

Fig. 1a

To create the Mean Annual Precipitation and elevation profiles in Fig. 1a, the following data were obtained for southeastern southern Africa:

(1) Worldclim v2 monthly mean precipitation data, 30 second (~1km2 resolution) (accessed September 19, 2019; http://worldclim.org/); and
(2) SRTM 1-arc second global (30m) resolution (accessed September 19, 2019 via earthexplorer.usgs.gov, DOI: /10.5066.F7PR7TFT).

ArcGIS Pro was then employed to: (1) sum monthly precipitation rasters from Worldclim to create a measure of Mean Annual Precipitation; (2) mosaic the SRTM tiles; and (3) extract values from elevation and precipitation rasters along the transect shown on the map in Fig. 1a using the Stack Profile tool.

Fig. 6a

To calculate minimum distances from the Lesotho rock-shelters to viable ostrich habitats underlain by Karoo Supergroup units of interest (Lower Stormberg, Beaufort and Ecc/Dwyka formations), the following data were obtained:

(1) Council for Geoscience's 'Simplified Geologic Map of South Africa, Lesotho and Swaziland' (1:1,000,000) (accessed July 2, 2019: http://www.geoscience.org.za/index.php/publication/downloadable-material).
(2) South Africa National Biodiversity Institute (SANBI) 2018 Vegetation Map of South Africa, Lesotho, and Swaziland (accessed August 2, 2019: http://bgis.sanbi.org/SpatialDataset/Detail/670).
(3) Ostrich distribution map of contemporary sightings, scanned from Sinclair et al.[41].

All data were then imported as individual layers into ArcGIS Pro, georeferenced where necessary, and converted to Africa Equidistant Conic projection. The simplified geologic map was queried for the Karoo Supergroup lithologies of interest. A mask was created for areas where ostriches are not endemic as discerned from both modern and historical observations. The mask combines (1) the southwest portion of the Sinclair et al. (2011) ostrich distribution map and (2) the Drakensberg Grassland, Sub-Escarpment Grassland, Sub-Escarpment Savanna, Zonal & Intrazonal Forests, and Indian Ocean Coastal Belt portions of the SANBI (bioregions) map. Identified minimum distances from site to each group by using Generate Near Table tool in ArcGIS Pro.

6. Key to site abbreviations in Fig. 5b

ADL	Adullam
BV	Belleview
BL	Bolahla
BW	Bonawe
BS	Borchers Shelter
CS	Collingham Shelter
CW	Colwinton
D1	Diamond 1
DL	Driel
ESH	eSinhlonhlweni
GH	Good Hope
GR	Grassridge
HM	Ha Makotoko
ISM	Ingane Shell Midden A
INK	iNkolimahashi
KTY	kwaThwaleyakhe
LH	Leliehoek
LT	Leqhetsoana
LIK	Likoaeng
LIP	Liphofung
MM	Malimong
MQ	Maqonqo
MB	Mbabane
MEL	Melikane
MW	Merino Walk
MG	Mgede
MZ	Mhlwazini
MS	Moshebi's Shelter
'M	'Muela
MZS	Mzinyashana 1
NP	Nkupe
NT	Ntloana Tšoana
OL	Oakleigh
PIT	Pitsaneng
RC	Ravenscraig
RK	Rooikrans
RCC	Rose Cottage Cave
SHE	Sehonghong
STA	Strathalan A
TB	Tandjesberg
TV	Te Vrede
TF	Tienfontein sites
TL	Tloutle
TFC	Tsakana Falls Cave
TW	Twyfelpoort
UB	Umbeli Belli
UMH	Umhlatuzana
VS	Ventershoek

SI References

1. S. S. Dornan, Notes on the Bushmen of Basutoland. *Trans S Afr Phil Soc* **18**, 437–450 (1909).

2. J. B. Wright, *Bushman Raiders of the Drakensberg 1840-1870* (University of Natal Press, Pietermaritzburg, South Africa, 1971).

3. S. Challis, Creolisation on the nineteenth-century frontiers of southern Africa: a case study of the AmaTola Bushmen in the Maloti-Drakensberg. *Journ S Afr Stud* **38**, 265–280 (2012).

4. P. Mitchell, S. Challis, A 'first' glimpse into the Maloti Mountains: the diary of James Murray Grant's expedition of 1873-74. *S Afr Hum* **20**, 399–461 (2008).

5. J. M. Orpen, A glimpse into the mythology of the Maluti Bushmen. *Cape Monthly Magazine* **9**, 1–13 (1874).

6. P. L. Carter, The prehistory of eastern Lesotho. PhD thesis, University of Cambridge, UK (1978).

7. J.C. Vogel, A. Fuls, E. Visser, Pretoria Radiocarbon dates III. *Radiocarbon* **28**, 1133–1172 (1986).

8. Z. Jacobs, R. G. Roberts, Testing times: old and new chronologies for the Howieson's Poort and Still Bay industries in environmental context. *S Afr Arch Soc Goodwin Series* **10**, 9-34 (2008).

9. Z. Jacobs, *et al.*, Ages for the Middle Stone Age of southern Africa: implications for human behavior and dispersal. *Science* **322**, 733–735 (2008).

10. B. A. Stewart, *et al.*, Afromontane foragers of the Late Pleistocene: site formation, chronology and occupational pulsing at Melikane Rockshelter, Lesotho. *Quat Int* **270**, 40–60 (2012).

11. J. M. Miller, Variability in ostrich eggshell beads from the Middle and Later Stone Age of Africa. PhD thesis, University of Alberta, Canada (2019).

12. A. W. Kandel, N. J. Conard, Production sequence of ostrich eggshell beads and settlement dynamics in the Geelbek Dunes of the Western Cape, South Africa. *J Archaeol Sci* **32**, 1711–1721 (2005).

13. B. A. Stewart, A. G. Parker, G. I. Dewar, M. W. Morley, L. F. Allott, Follow the Senqu: Maloti-Drakensberg paleoenvironments and implications for early human dispersals. In *Africa From MIS 6–2*, eds Jones, S. A. & Stewart, B. A. (Springer, Dordrecht, Netherlands), 247–272 (2016).

14. C. Bronk Ramsey, Bayesian analysis of radiocarbon dates. *Radiocarbon* **511**, 337–360 (2009).

15. A. G. Hogg, *et al.*, SHCal13 southern hemisphere calibration, 0-50,000 years cal BP. *Radiocarbon* **55**, 1889–1903 (2013).

16. W. T. Bell, D. W. Zimmerman, The effect of HF etching on the morphology of quartz inclusions for thermoluminescence dating. *Archaeometry* **20**, 63–65 (1978).

17. V. Mejdahl, Thermoluminescence dating: beta-dose attenuation in quartz grains. *Archaeometry* **21,** 61–72 (1979).

18. J. R. Prescott, J. T. Hutton, Cosmic ray contributions to dose rates for luminescence and ESR dating:

large depths and long-term time variations. *Radiat Meas* **23**, 497–500 (1994).

19. M. A. Smith, J. R. Prescott, M. J. Head, Comparison of ^{14}C and luminescence chronologies at Puritjarra rock shelter, central Australia. *Quat Sci Rev* **16**, 299–320 (1997).

20. M. L. Readhead, Thermoluminescence dose rate data and dating equations for the case of disequilibrium in the decay series. *Nucl Tracks and Radiat Meas* **13**, 197–207 (1987).

21. R. F. Galbraith, R. G. Roberts, G. M. Laslett, H. Yoshida, H., J. M. Olley, Optical dating of single and multiple grains of quartz from Jinmium rock shelter, northern Australia: part I, experimental design and statistical models. *Archaeometry* **41**, 339–364 (1999).

22. J. D. Lewis-Williams, D. G. Pearce, *San Spirituality: Roots, Expression and Social Consequences* (AltaMira Press, Walnut Creek, CA, 2005).

23. P. V. Vinnicombe, Basotho oral knowledge: the last Bushman inhabitants of the Mashai District, Lesotho. In *The Eland's People: New Perspectives in the Rock Art of the Maloti-Drakensberg Bushmen. Essays in Memory of Patricia Vinnicombe*, eds Mitchell, P. J. & Smith, B. W. (Wits University Press, Johannesburg, South Africa), pp. 165–191 (2009).

24. P. J. Mitchell, Making history at Sehonghong: Soai and the last Bushman occupants of his shelter. *S Afr Hum* **22**, 147–168 (2010).

25. P. L. Carter, J. C. Vogel, The dating of industrial assemblages from stratified sites in eastern Lesotho *Man* **9**, 557–570 (1974).

26. P. L. Carter, P. J. Mitchell, P. V. Vinnicombe, *Sehonghong: The Middle and Later Stone Age Industrial Sequence from a Lesotho Rockshelter*. (British Archaeological Reports International Series, Oxford, 1988).

27. P. J. Mitchell, The late Quaternary of the Lesotho highlands, southern Africa: preliminary results and future research at Sehonghong Shelter. *Quat Int* **33**, 35–44 (1996).

28. E. Loftus, B. A. Stewart, G. I. Dewar, J. A. Lee-Thorp, Stable isotope evidence of late MIS 3 to middle Holocene palaeoenvironments from Sehonghong Rockshelter, eastern Lesotho. *J Quat Sci* **30**, 805–816 (2015).

29. I. Plug, P. J. Mitchell, Sehonghong: hunter-gatherer utilization of animal resources in the highlands of Lesotho. *Ann Transvaal Mus* **45**, 1–23 (2008).

30. P. J. Mitchell, Understanding the MSA/LSA transition: the pre-20,000 BP assemblages from new excavations at Sehonghong rock-shelter, Lesotho. *S Afr Field Archaeol* **3**,15–25 (1994).

31. P. J. Mitchell, Revisiting the Robberg: new results and a revision of old ideas at Sehonghong rock-shelter, Lesotho. *S Afr Archaeol Bull* **50**, 28–38 (1995).

32. P. J. Mitchell, The late Quaternary of the Lesotho highlands, southern Africa: preliminary results and future research at Sehonghong Shelter. *Quat Int* **33**, 35–44 (1996).

33. P. J. Mitchell, Sehonghong: the late Holocene assemblages with pottery. *S Afr Archaeol Bull* **51**, 17–25 (1996).

34. A. K. Horsbugh, J. V. Moreno-Mayar, A. L. Gosling, Revisiting the Kalahari debate in the highlands: ancient DNA provides new faunal identifications at Sehonghong, Lesotho. *Azania: Archaeol. Res. in Africa* **51**, 295–306 (2016).

35. J. Pargeter, E. Loftus, P. J. Mitchell, New ages from Sehonghong rockshelter: implications for the late Pleistocene occupation of highland Lesotho. *J Archaeol Sci: Reports* **12**, 307–315 (2017).

36. J. M. McArthur, R. J. Howarth, T. R. Bailey, Strontium Isotope Stratigraphy: LOWESS version 3: best fit to the marine Sr-isotope curve for 0–509 Ma and accompanying look-up table for deriving numerical age. *J Geol* **109**,155–170 (2001).

37. S. de Villiers, J. S. Compton, M. Lavelle, The strontium isotope systematics of the Orange River, southern Africa. *S Afr J Geol* **103**, 237–248 (2000).

38. J. D. Gleason *et al.*, Ichthyolith strontium isotope stratigraphy of a Neogene red clay sequence: Calibrating eolian dust accumulation rates in the central North Pacific. *Earth Planet. Sci. Lett.* **202**, 625–636 (2002).

39. A. M. Stancin, *et al.*, Radiogenic isotopic mapping of late Cenozoic eolian and hemipelagic sediment distribution in the east-central Pacific. *Earth Planet. Sci. Lett.* **248**, 840–850 (2006).

40. RStudio Team. RStudio: Integrated Development for R. RStudio, Inc., Boston, MA URL http://www.rstudio.com/ (2015).

41. I. Sinclair, P. Hockey, W. Tarboton, P. Ryan, *SASOL Birds of Southern Africa (Fourth edition)* (Struik Nature, Cape Town, South Africa, 2011).